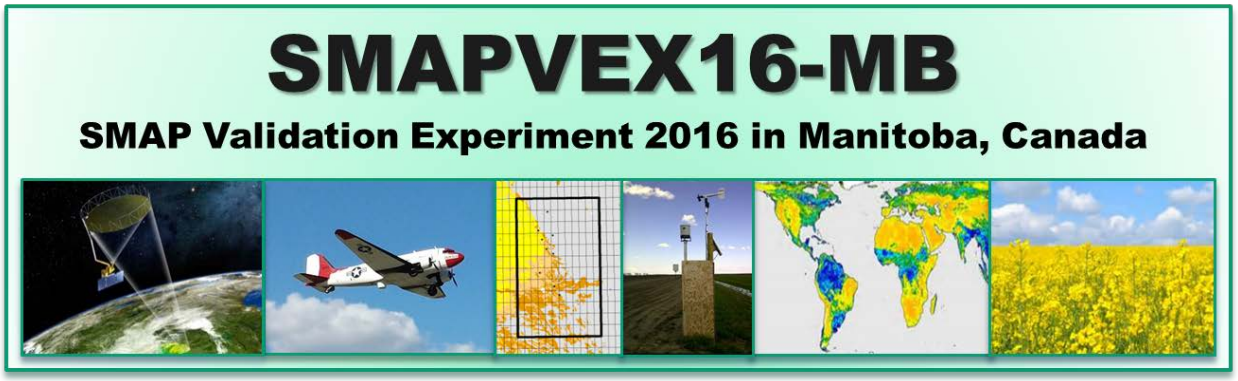

SMAPVEX16 Database Report

January 31, 2017

Heather McNairn[1*], Tom J. Jackson[2], Jarrett Powers[3], Stephane Bélair[4], Aaron Berg[5], Paul Bullock[6], Andreas Colliander[7], Michael H. Cosh[2], Seung-Bum Kim[7], Ramata Magagi[8], Anna Pacheco[1], Amine Merzouki[1], Mehdi Hosseini[1], Krista Hanis-Gervais[6]

[1] Agriculture and Agri- Food Canada, Science and Technology Branch, Ottawa, ON K1A 0C6, CANADA
[2] USDA-ARS Hydrology and Remote Sensing Lab, Beltsville, MD 20705, USA
[3] Agriculture and Agri- Food Canada, Science and Technology Branch, Winnipeg, MB R3C 3G7, CANADA
[4] Environment Canada, Meteorological Research Branch, Dorval, QC H9P 1J3, CANADA
[5] University of Guelph, Department of Geography, Guelph, ON N1G 2W1, CANADA
[6] University of Manitoba, Department of Soil Science, Winnipeg, MB R3T 2N2, CANADA
[7] Jet Propulsion Laboratory, Pasadena, CA 91109, USA
[8] Université de Sherbrooke, Département de géomatique appliquée, Sherbrooke, QC J1K 2R1, CANADA

*corresponding author: Agriculture and Agri- Food Canada, Science and Technology Branch, Ottawa, ON K1A 0C6, CANADA
heather.mcnairn@agr.gc.ca

Table of Contents

Table of Figures

List of Tables

1. Study Area

The Red River Watershed of southern Manitoba provides a mix of land covers, although land use is dominated by annual cropping. This region has been used in decades of soil moisture research, dating back to the early 1990s when the Jet Propulsion Laboratory (JPL) flew their AIRSAR airborne sensor over the region (1993) and when Altona, Manitoba served as a research site for SIR-C (1994). Subsequently, southern Manitoba has been used extensively to develop and validate soil moisture retrievals using Canada's RADARSAT satellites. This research led Agriculture and Agri-Food Canada (AAFC) to install permanent in situ soil moisture stations in the La Salle and Boyne River watersheds, part of the larger Red River basin.

1.1 General description

The Canadian Red River Watershed (Figure 1) is a watershed of extremes in soil moisture. For example, according to the 2008-2009 Annual Report from the Manitoba Agricultural Services Corporation drought and excessive heat have historically (1960-2007) accounted for 37% of reported crop losses, while excessive moisture was responsible for 36% of losses. The watershed is characterized largely by agricultural land use with a wide range of crop and soil conditions. Crops include forage, pasture, canola, flaxseed, sunflower, soybean, corn, barley, spring wheat, winter wheat, rye, oats, canary seed, potatoes, and field peas. The typical crop rotation is a cereal crop alternating with oilseed\pulse crops. Typical field sizes range from 20-30 to 50-60 hectares. Annual crop type mapping for the entire Red River Watershed, via remote sensing techniques, is completed by AAFC. It is also important to note that this is a shared watershed with the U.S. Three-quarters of the Red River Watershed lies on the U.S. side of the border.

AAFC installed permanent soil moisture monitoring stations (Real-time In-situ Soil Monitoring for Agriculture or RISMA) in Manitoba, in two phases. Nine stations were installed near the towns of Carman and Elm Creek, located 80 km southwest of the city of Winnipeg in 2011. Three other stations were installed in the Sturgeon Creek watershed in 2013, located immediately northwest of Winnipeg. The stations in Carman-Elm Creek are situated in the La Salle and Boyne River watersheds which are part of the larger Red River basin. The Sturgeon Creek watershed is part of the larger Assiniboine River basin. These areas are part of Canada's Prairie/Boreal Plain Ecozone and were chosen to capture the diverse soil moisture conditions in the Manitoba portion of the Red River and lower Assiniboine River basins. The Carman-Elm Creek site has an excellent contrast in soil properties from west (fine clay soils) to east (coarser and better drained soils). The watershed is approximately 60 km (east-west) by 10 km (north-south).

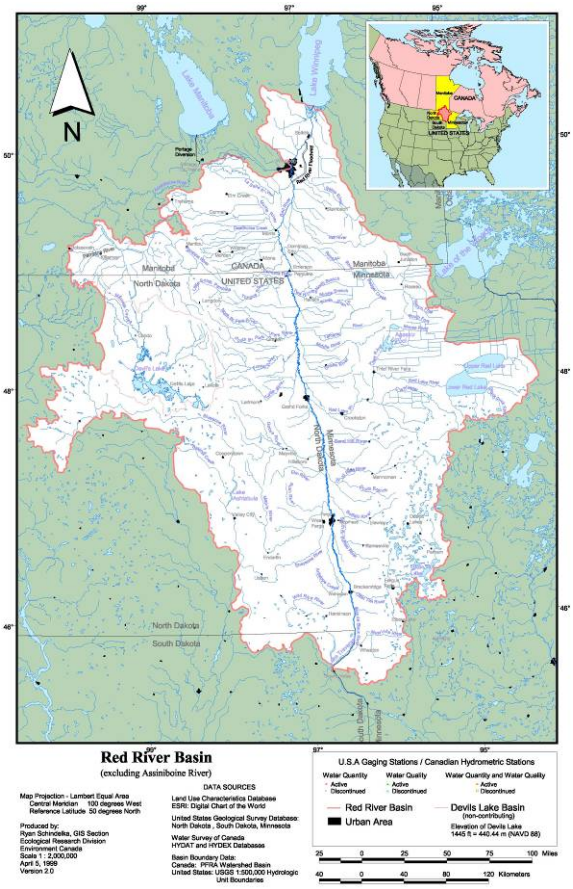

Figure 1. Extent of the Red River Watershed
Approximately 25% of the watershed falls within Canada, with the remainder of the watershed residing within Minnesota, North Dakota and South Dakota, U.S.A

1.2 Intensive sample site description

The Soil Moisture Active Passive Validation Experiment 2016 for Manitoba (SMAPVEX16-MB) intensive sample site has been shifted east and south of the location of the 2012 experiment. The 2016 study site corresponds to the 36-km SMAP pixel used in the calibration and validation exercise during the pre- and post-launch of SMAP (Figure 2).

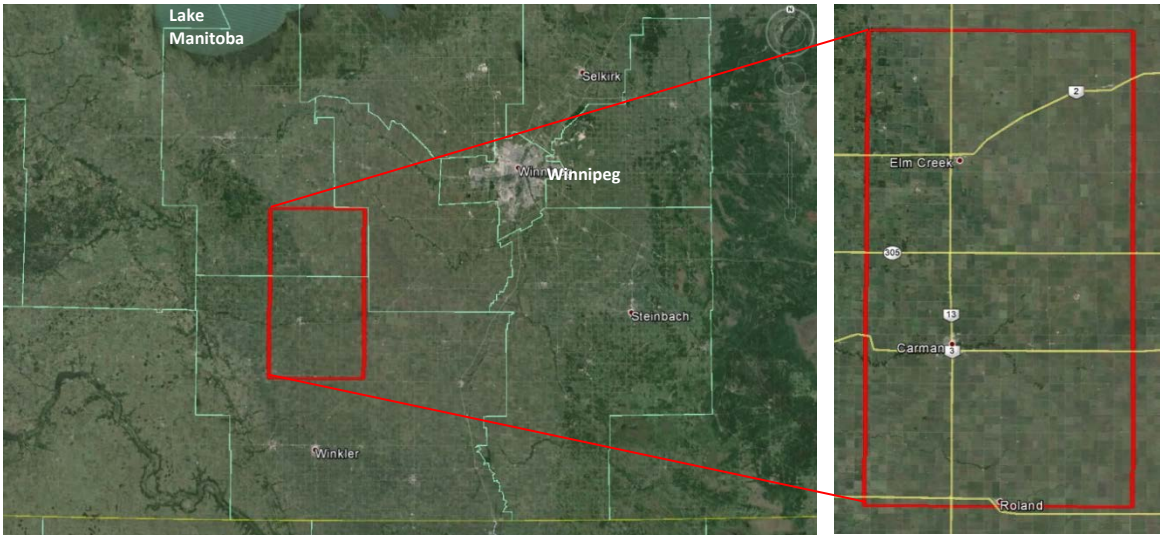

Figure 2. Location of the SMAPVEX16 intensive site relative to the city of Winnipeg (Manitoba)

The site dimensions are approximately 26 km x 48 km. According to the Manitoba Agricultural Services Corporation (MASC) Crop Insurance data, more the 85% of the area is dominated by the following annual crops: canola, soybeans, wheat, corn oats, winter wheat and beans. Only a small fraction (< 5%) is under grassland and pasture. The crop type distribution within the SMAP region of interest is described in Table 1. Figure 3 provides the 2015 crop map generated by AAFC.

Table 1. 2015 crop type distribution within the SMAP pixel

Crop Type	Percent Area (%)
Soybeans	29.88
Spring wheat	24.12
Canola/Rapeseed	18.24
Corn	8.28
Oats	6.92
Deciduous Forest	2.29
Grassland	1.96
Beans	1.50
Winter wheat	1.41
Sunflower	1.12
Others	4.28

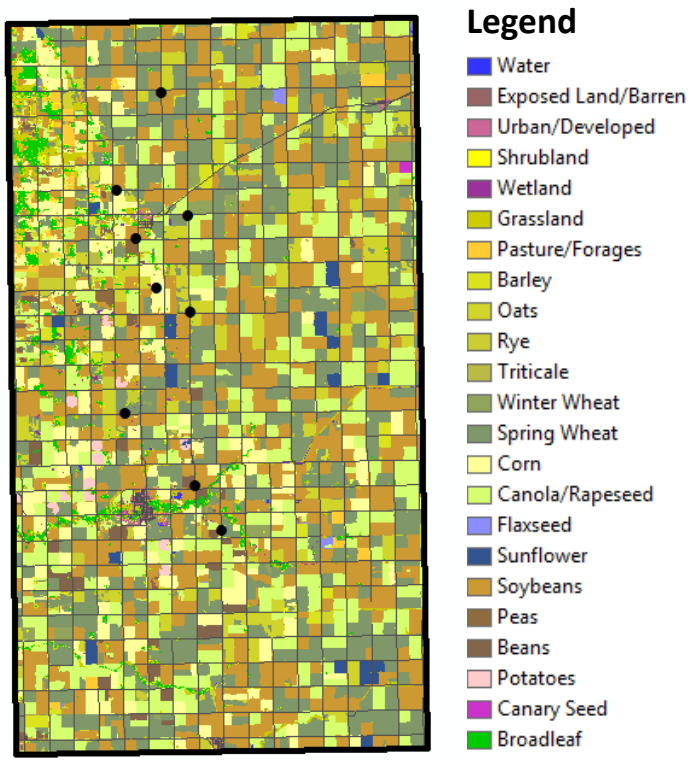

Figure 3. The 2015 crop map for the SMAPVEX16-MB intensive sample site
The AAFC RISMA sites are identified as black dots

2. In Situ Monitoring of Soil and Meteorological Conditions

2.1 AAFC In Situ Soil Moisture Network (RISMA)

In 2011, AAFC began installing an in situ soil moisture monitoring network in and around Carman-Elm Creek. The RISMA (Real-time In-situ Soil Monitoring for Agriculture) network, was established to provide a direct source of near-real time information on soil moisture conditions in an agriculturally risk-prone watershed, and to provide a data set that can be used holistically with remotely-sensed and modelled data products for calibration and validation of models. The network was designed to capture the maximum soil variability within the Red River watershed, with the specific location of the sensors established along a gradient of soil texture classes (Figure 4).

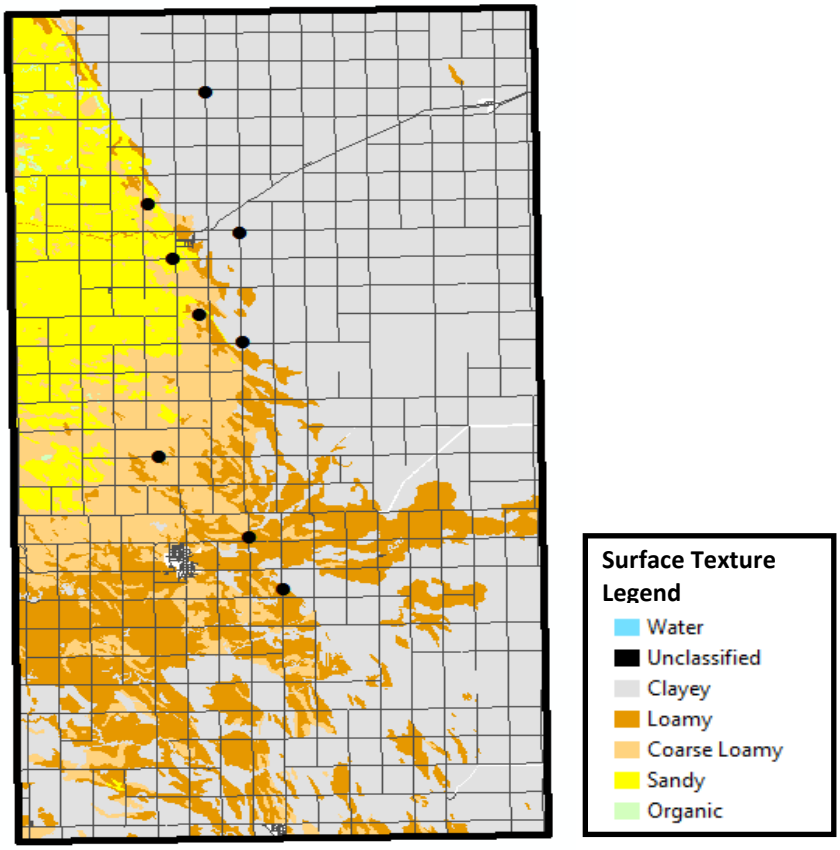

Figure 4. Location of the AAFC RISMA network in Manitoba (black dots)
The backdrop image shows clay dominated soils on the eastern portion of the watershed and sandier soils on the western portion of the watershed.

The RISMA network consists of nine in situ monitoring stations distributed proportionally to be representative of the different soil texture classes. Sites were selected based on soil texture variability, willingness to cooperate from local producers and soil survey by regional soil experts. Each station is instrumented with Stevens' Hydra Probes which measure soil dielectric, soil moisture and soil temperature, with triplicate measurements of the soil properties at each depth. This redundancy was applied to ensure critical variables would continue to be captured in the event of sensor failure, and to provide an indication of the within site variability in moisture conditions. Soil moisture and temperature are measured horizontally at depths of 5, 20, 50 and 100 cm, with an additional three probes place vertically at the surface to capture integrated surface soil moisture over a 6cm depth (Figure 5). Meteorological observations are also captured at each station including liquid precipitation, air temperature, relative humidity, wind speed and wind direction. Sites are instrumented with Hoskin Scientific tipping bucket rain gauges, and Geneq sensors for all other meteorological parameters, and powered by solar panels and batteries (Figure 6). Data are recorded on Campbell Scientific CR1000-XT data loggers and transmitted to AAFC through Raven X modems on the hour mark. Measurements are collected on a 15-minute time frequency for all variables. Data can be viewed and downloaded online in near real-time by accessing the following link: http://aafc.fieldvision.ca./.

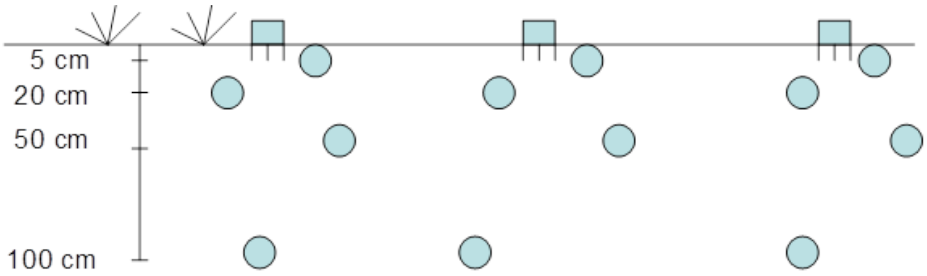

Figure 5. Schematic of probe location within each soil pit for AAFC RISMA sites

Figure 6. Site installation for AAFC in situ soil moisture sites

All AAFC sites are located within or on the edge of cultivated agricultural fields, with the system set up to capture data (when valid) year round without removal of equipment required due to land management activities. During installation, soil cores were collected at the location of each probe installation and preserved for site specific calibration, soil texture and bulk density analysis. Site specific soil moisture dielectric conversion models have been developed using field calibration (Ojo et al., 2015). These calibration models have been applied to each sensor to obtain higher accuracy soil moisture values.

2.2 SMAPVEX16-MB Temporary In Situ Soil Moisture Network

Previous work has demonstrated the utility of installing temporary networks to increase the spatial coverage of a network. This provides a scaling period which will enable a network manager to provide a more accurate error statistic for the network and scaling functions for improving the representative

character of the in situ network. In May and after the completion of spring seeding, temporary soil moisture stations (Figure 7) were deployed within SMAPVEX16-MB fields. Stations remained in place though out the campaign and were removed in August prior to harvest. These stations recorded hourly soil moisture and soil temperature data.

Figure 7. A USDA temporary station with a solar panel and CR206 logger at site 1 of a canola field A Stevens Hydra Probe and a CS655 reflectometer are installed at a depth of 5 cm to mimic the long term in situ station.

A total of 50 stations were deployed within the study area, one for every study field. Each station was installed at the first sample site (site 1; refer to section 4 for a description of site locations). 40 of these stations were equipped with one Stevens Hydra-Probe II and one Campbell Scientific 655 TDR soil moisture probe installed horizontally at 5 cm. A second Hydra-Probe was installed in a vertical orientation at the surface. In addition, 16 of the 40 stations were equipped with Hydrologic Services TB4 tipping buckets to measure precipitation.

The remaining 10 stations were equipped with two Stevens Hydra-Probe II probes; one at the horizontal 5 cm and the other in a vertical orientation at the surface. Data from all the temporary stations were logged hourly.

2.3 Other Agriculture Weather Networks

2.3.1 Manitoba Agriculture, Food and Rural Development (MAFRD) Agriculture Weather Network

Manitoba Agriculture, Food and Rural Development (MAFRD) provide weather-related information and value-added tools to producers in Manitoba via the Manitoba Agriculture Weather Program (MAWP). The province of Manitoba currently operates approximately 63 automated near real-time weather stations. The program will undergo an expansion in the next several years with the addition of another 30 stations. The expansion will include retrofitting all current stations with soil moisture and temperature monitoring capability at 5 and 20 cm depths. The University of Manitoba, through Dr. Paul Bullock, has contributed Stevens Hydra probes for soil moisture monitoring at the Treherne, Carman and St. Adolphe locations of this network. A map (Figure 8) below demonstrates the distribution of the network in the south central portion of Manitoba.

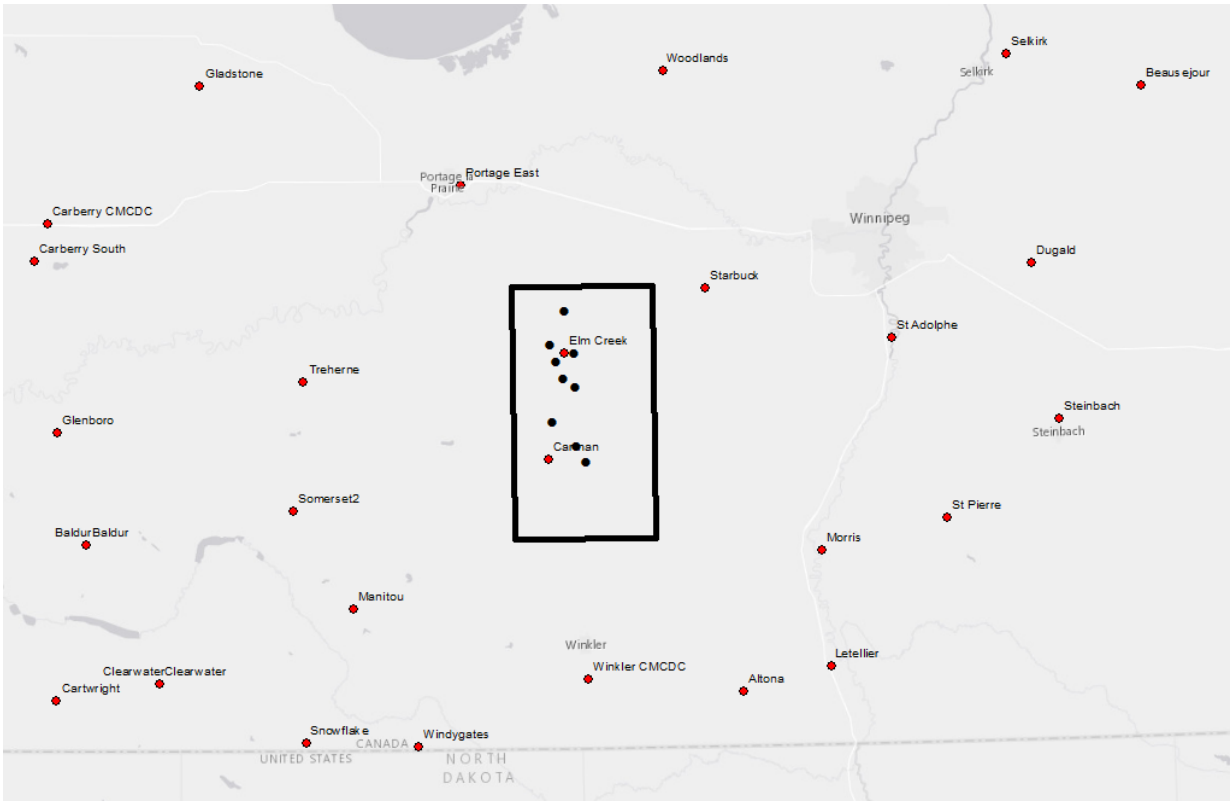

Figure 8. Distribution of the Manitoba Agriculture, Food and Rural Development (MAFRD) agriculture weather monitoring stations in the south central portion of Manitoba

The Carman (49.498 N, -98.030 W) and Elm Creek stations are of particular interest given that they are located within the SMAP footprint. The Carman station collects various meteorological parameters including air temperature, relative humidity, liquid precipitation, solar radiation, and wind speed and direction. This station is also instrumented with single Stevens Hydra probes at various depths: 5, 20, 50

and 100 cm depths (Figure 5), which outputs soil moisture (default calibration), soil temperature, imaginary and real dielectric permittivity. Similar to the RISMA network, the Carman station is equipped with a Campbell Scientific CR1000 data logger where data are recorded and sent wirelessly to the server via a modem. The stations' sensors record data every 5 seconds and these data are then processed into 15-minute data, hourly data and daily (24 hour) data. Data from the stations are currently being shared with the public in the form of an hourly-updated image file that shows current conditions (http://www.gov.mb.ca/agriculture/weather/current-ag-weather-conditions.html) as well as basic tabular output of a few variables (http://tgs.gov.mb.ca/climate/DailyReport.aspx).

2.3.2 Environment Canada Weather Network

Several meteorological stations are located within the agricultural regions of Manitoba, which are part of the Environment Canada weather network. Most stations record typical meteorological variables including air temperature, total precipitation, wind speed and direction, and relative humidity, while others collect additional data on dew point temperature, net radiation, snow accumulation and soil temperature. Environment Canada data can be downloaded from their website (http://climate.weatheroffice.gc.ca/climateData/canada_e.html) by locating specific climate stations through their query tool. The map below (Figure 9) illustrates the distribution of the weather stations established by Environment Canada in southern central Manitoba.

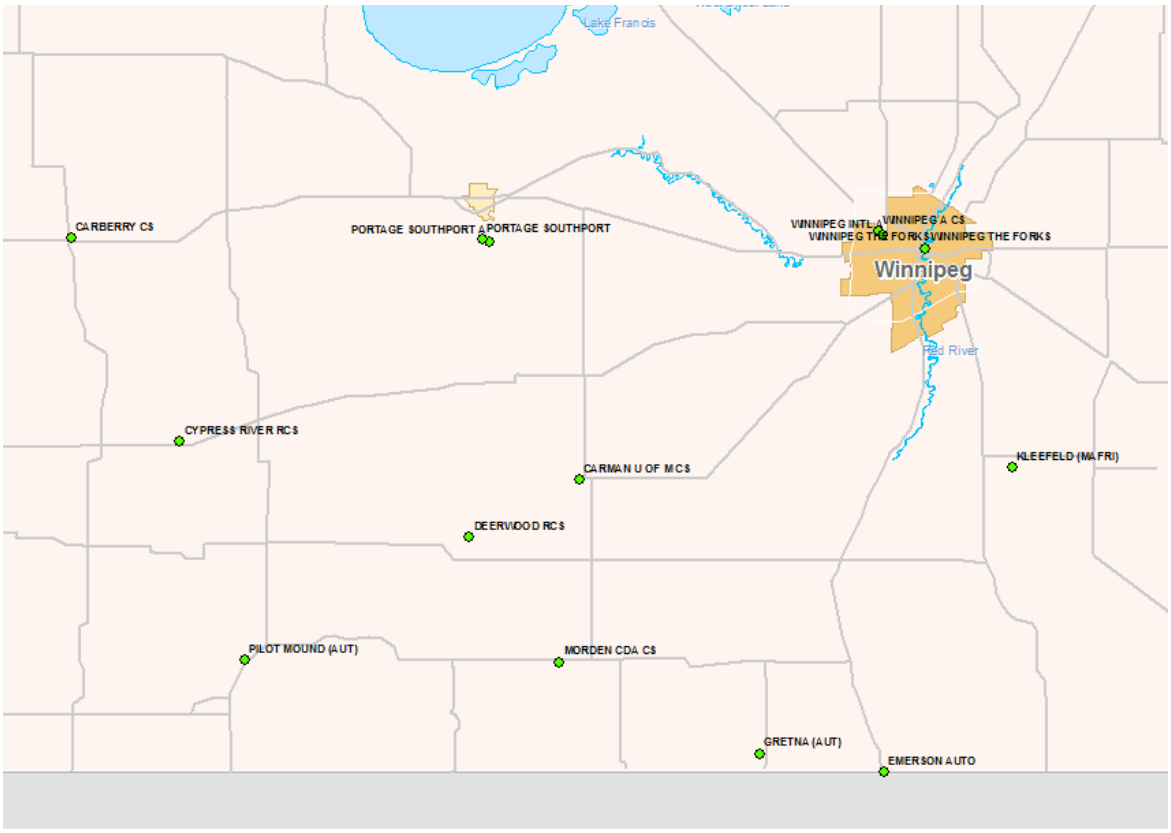

Figure 9. Distribution of the Environment Canada weather stations located in southern central Manitoba

3. Ancillary Datasets

3.1 Digital Elevation Modelled Data

Digital elevation model (DEM) data for the area are available from a number of sources including the Natural Resources Canada's (NRCan) products such as the Canadian Digital Elevation Data (CDED) and the Canadian Digital Elevation Model (CDEM). Other DEMs were generated from specific satellite missions including the Advanced Spaceborne Thermal Emission and Reflection Radiometer (ASTER) Global Digital Elevation Model Version 2 (GDEM V2) and the Shuttle Radar Topography Mission (SRTM).

The CDED is produced by NRCan and is extracted from the hypsographic and hydrographic elements of the National Topographic Data Base (NTDB). The CDED data are available in 23 metre (1:50 000) and 93 metre (1:250 000) spatial resolutions, with 10m vertical accuracy for the 23-m dataset. Data are freely available and can be downloaded from Natural Resources Canada's GeoGratis portal (http://www.nrcan.gc.ca/earth-sciences/geography/topographic-information/free-data-geogratis/11042). The CDED product is however no longer supported by NRCan and elevation data users are encouraged to employ the CDEM instead. The CDEM stems from the existing CDED but elevation information were derived from either ground or reflective surface elevations. A mosaic can be obtained for a pre-defined or user-defined extent, where coverage and resolution of the mosaic will vary on the latitude and to the extent of the requested area. Derived products such as slope, shaded relief and colour shaded relief maps can also be generated on demand. Various spatial resolutions can be obtained for the CDEM including 20-, 50-, 90-, 200- and 400-m.

The Ministry of Economy, Trade, and Industry (METI) of Japan and the United States National Aeronautics and Space Administration (NASA) jointly produced the ASTER GDEM V2 dataset. This product was released in 2011 and is an improved version of the original product ASTER GDEM (released in 2009) which was generated using stereo-pair images collected by the ASTER instrument onboard Terra. The GDEM V2 has improved coverage and reduced occurrence of artifacts. The refined production algorithm provides enhanced spatial resolution, improved horizontal and vertical accuracy, and refined water body coverage and detection. The ASTER GDEM V2 is available in GeoTIFF format at 30-m spatial resolution with a 7- to 14-m vertical accuracy (Figure 10). The product can be downloaded free of charge to users worldwide from the Land Processes Distributed Active Archive Center (LP DAAC).

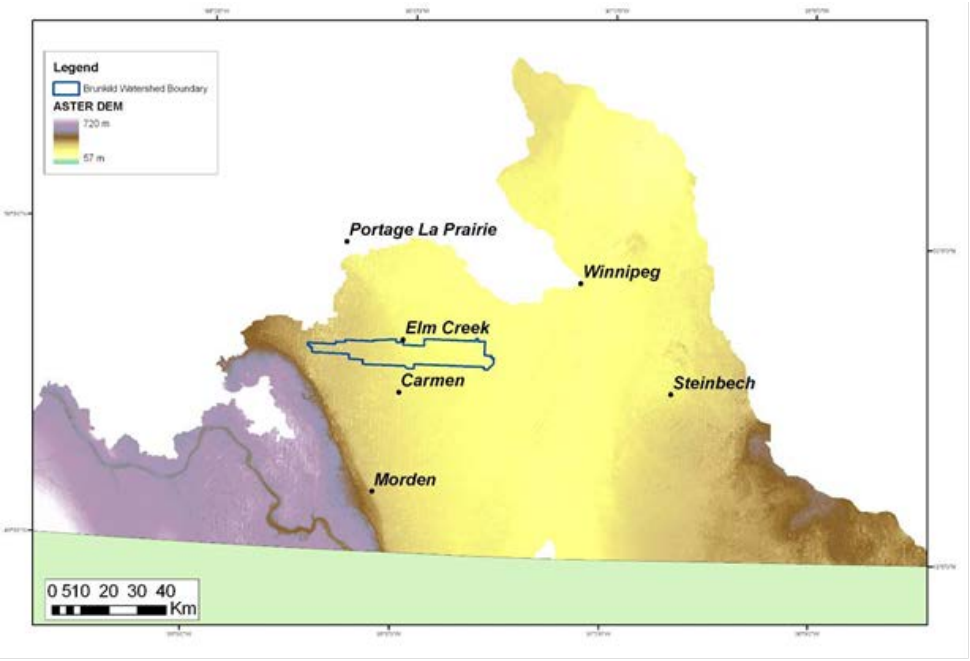

Figure 10. Digital Elevation Model data from the ASTER GDEM project for the Red River Watershed

The Shuttle Radar Topography Mission has recently released an enhanced 30-m DEM in late 2015. This mission was an international effort led in 2000 by the U.S. National Geospatial-Intelligence Agency (NGA) and NASA. Interferometric synthetic aperture radar was used to obtain elevation data. Lower-resolution elevation data at 90-m were first released in 2003 for several parts of the world. The elevation data are configured into tiles, each covering one degree of latitude and one degree of longitude, labeled according to their south western corners. The absolute accuracy of the DEM is less than 16-m (whereas the relative accuracy is less than 10-m). The data are available for download from the USGS EROS Data Center (http://eros.usgs.gov/).

3.2 Soils Data

Soils data for the study area was produced from the Canada-Manitoba Soil Survey Report D60, Soils of the Rural Municipalities of Grey, Dufferin, Roland, Thompson & Part of Stanley. The report is mapped at a detailed 1:20,000 scale and can be accessed from the Canadian Soil Information Service (CanSIS) website at http://sis.agr.gc.ca/cansis/publications/surveys/mb/index.html. Geospatial data provides further information on taxonomy, soil properties (soil texture, internal drainage, salinity, permanent wilting point, field capacity, pH, other chemical properties) and landscape properties (slope steepness, slope length, stoniness, erosion). These datasets can be downloaded at http://sis.agr.gc.ca/cansis/nsdb/dss/v3/index.html.

Considering the SMAPVEX16-MB study site (Figure 4), clay and fine loamy soils account for approximately 76.5% of the study area; coarse loamy and sand soils for 13.5%.

3.3 Land Cover and Crop Data

AAFC has developed a Decision Tree-based methodology to map crop types over Canadian agricultural landscapes by integrating optical and synthetic aperture radar (SAR) imagery (Figure 11). In 2009, the

Earth Observation Team of the Science and Technology Branch (STB) at AAFC began delivering annual crop type digital maps on an operational basis over the Prairies. Starting in 2011, the crop mapping activity has been extended to other provinces in support of a national crop inventory. The approach has consistently generated a crop inventory that meets the overall target accuracy of at least 85% at a 30-m spatial resolution (56m in 2009 and 2010). The annual crop inventories are available in GeoTIF format and typically delivered before April following the growing season. Land cover data are also included in the crop inventory dataset, which includes annual and perennial agricultural land, as well as native grassland, forest, wetland and urban areas within the agricultural extent. The data are available on the Government of Canada Open Portal at the following link: http://open.canada.ca/data/en/dataset/ba2645d5-4458-414d-b196-6303ac06c1c9.

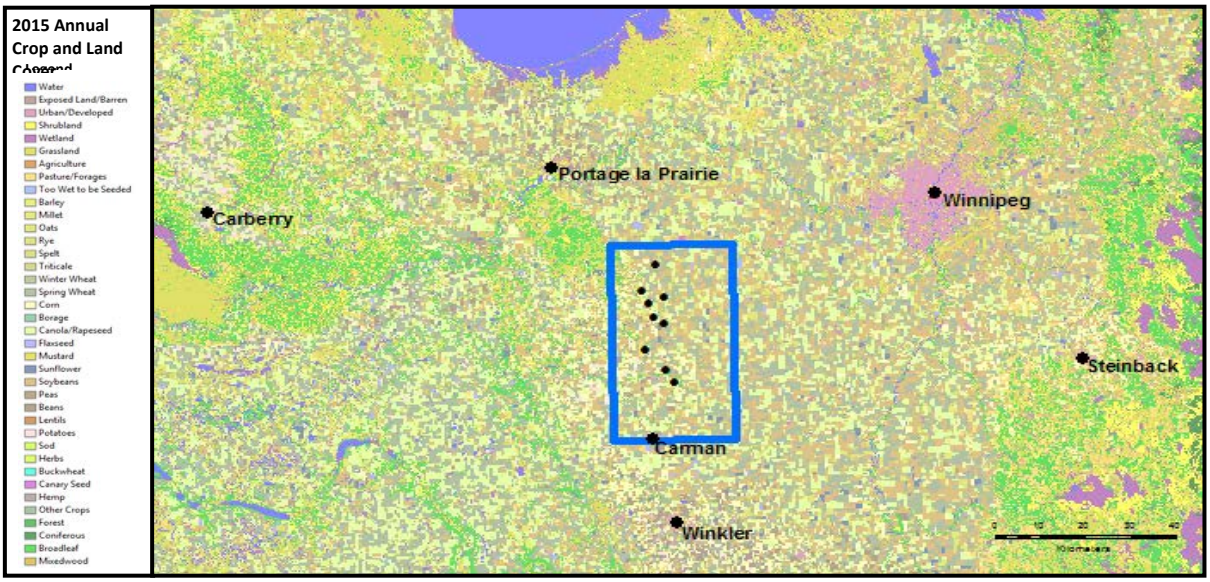

Figure 11. Agricultural land cover/annual crop types for central southern Manitoba
The SMAPVEX16-MB intensive sample site is outlined in blue and the AAFC RISMA sites are identified as black dots.

4. Field and Sampling Locations

In total, 50 fields (Figure 12) were selected for sampling during SMAPVEX16-MB. Of these 50 fields, 21 fields were also sampled during the SMAPVEX12 experiment. Fields were selected to be representative of both crop and soil conditions within the SMAP pixel. Manitoba Crop Insurance and the AAFC Annual Crop Inventory were analyzed to look at cropping trends in the study area. Soybeans, wheat and canola accounted for approximately 70% of crops grown in the study area (2 and 5 year average). Other crops include corn, oats, field beans and forages. Once potential fields were identified permissions were sought from landowners. For landowners in agreement, contracts were signed to grant access to the fields and to provide producers with financial compensation.

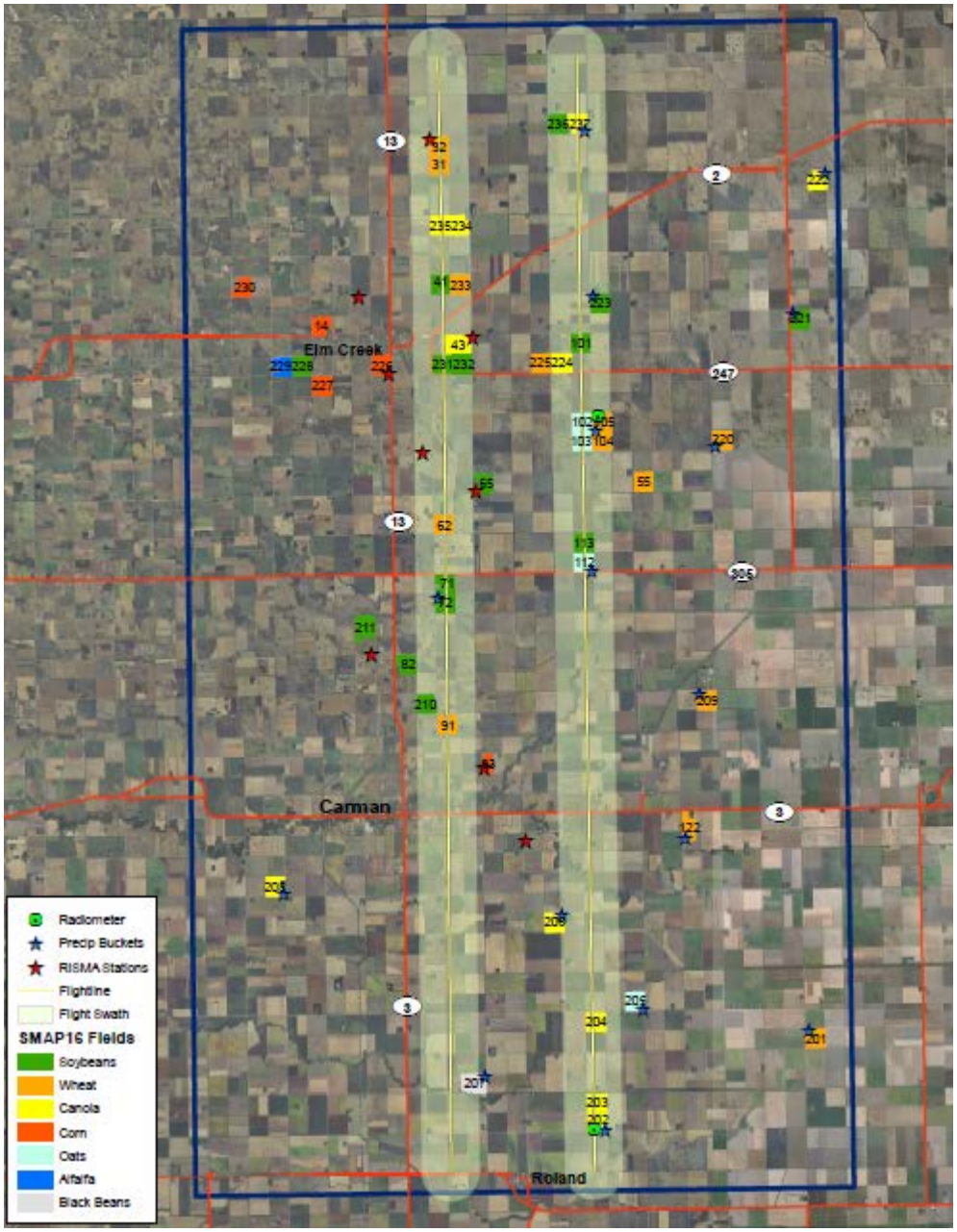

Figure 12. Location of the 50 SMAPVEX16 sample fields

In Figure 12, the locations of RISMA stations are marked (red stars) as well as those of additional rain buckets (blue stars). The type of crop grown on each SMAPVEX16 field is colour coded, but also documented in Table 2. Yellow marks PALS flight lines.

Table 2. Crop and soil textures for the 50 SMAPVEX16-MB fields

Field ID	Crop Type	Soil Texture	Field ID	Crop Type	Soil Texture
14	Corn	Sand	205	Oats	Clay
31	Wheat	Clay	206	Canola	Fine Loam
32	Wheat	Clay	207	Black Beans	Fine Loam
41	Soybeans	Clay	208	Canola	Fine Loam
43	Canola	Clay	209	Wheat	Fine Loam
55	Wheat	Clay	210	Soybeans	Coarse Loam
62	Wheat	Coarse Loam	211	Soybeans	Coarse Loam
65	Soybeans	Clay	220	Wheat	Clay
71	Soybeans	Coarse Loam	221	Soybeans	Clay
72	Soybeans	Coarse Loam	222	Canola	Clay
82	Soybeans	Coarse Loam	223	Soybeans	Clay
91	Wheat	Coarse Loam	224	Canola	Clay
93	Corn	Fine Loam	225	Wheat	Clay
101	Soybeans	Clay	226	Corn	Sand
102	Oats	Clay	227	Corn	Sand
103	Oats	Clay	228	Soybeans	Sand
104	Wheat	Clay	229	Alfalfa	Sand
105	Wheat	Clay	230	Corn	Sand
112	Oats	Clay	231	Soybeans	Fine Loam & Clay
113	Soybeans	Clay	232	Soybeans	Clay
122	Wheat	Fine Loam & Clay	233	Wheat	Clay
201	Wheat	Clay	234	Canola	Clay
202	Canola	Fine Loam	235	Canola	Clay
203	Canola	Fine Loam	236	Soybeans	Clay
204	Canola	Clay	237	Canola	Clay

Soil moisture varies significantly across the landscape. In order to capture soil moisture conditions representative of each of the SMAPVEX16-MB fields, multiple sampling was required. Thus for each field, soil moisture was measured at sixteen sampling points, with three replicate measurements at each of these sample points. For ease of access and navigation, these 16 sample points were arranged in two transects of 8 points running parallel to crop row direction (Figure 13). Crews entered the field at site 1, then sampled up to site 8, traversing over to site 9 and sampling back to site 16.

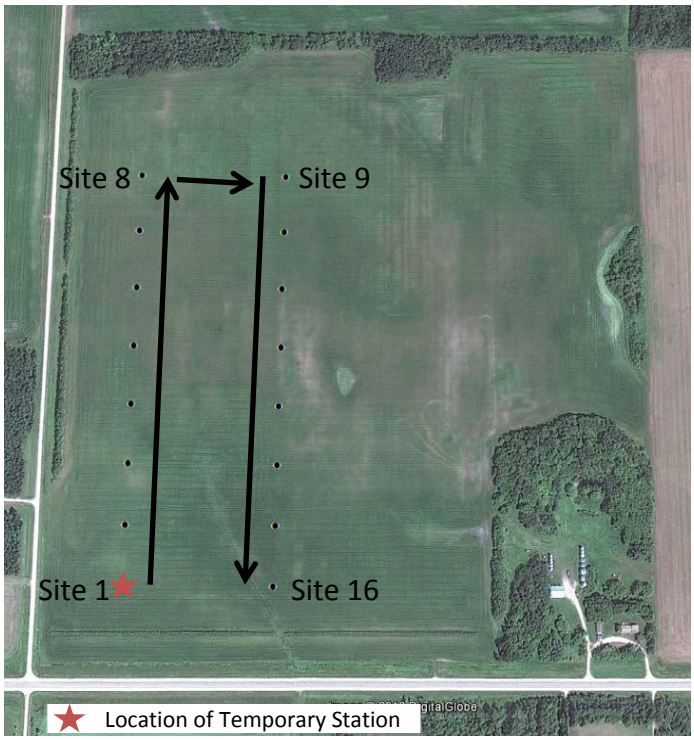

Figure 13. Location of parallel transects in SMAPVEX16-MB fields

Aerial photos were used to position transects to avoid anomalies in the fields, such as field drains. The location of each sample point was pre-loaded into handheld GPS devices so that crews could easily navigate to each point. For the most part, the positioning of the transects meant that moisture conditions were measured along the full extent of the field. Transects were also positioned to avoid edge effects were soil and vegetation conditions may not be typical of the field due to management practices. The sampling grid was located 100m from the edge of the field (Figure 14). Points were 75m apart with 200m between the two transects rows.

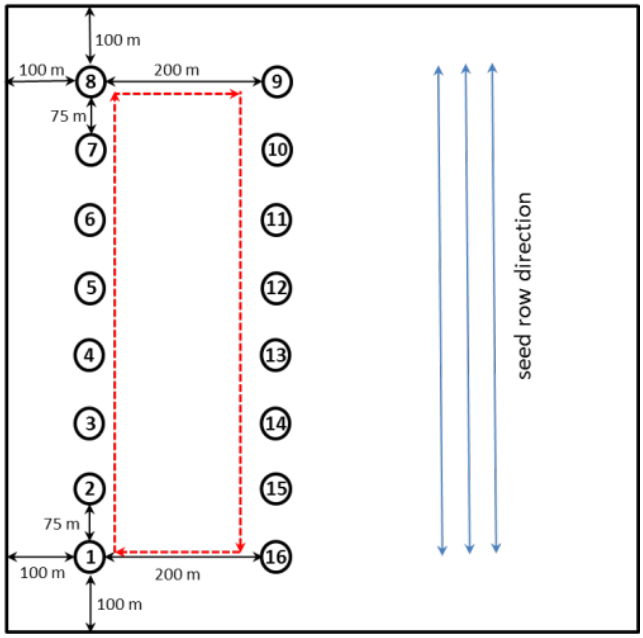

Figure 14. Spacing between soil moisture sampling points and from edge of field

5. SMAPVEX Intensive Observing Periods (IOPs)

While overall performance of the SMAP L2SMP (Chan et al., 2016) has been good, larger errors have been observed in some calibration/validation sites dominated by annual crop land. These include both the South Fork (Iowa) and Carman (Manitoba) sites. Given these findings, validation experiments were initiated over two intensive observing periods (IOPs) for each of these two sites (Iowa-IA and Manitoba-MB). The first IOP was designed to capture soil and crop conditions early in the season and the second to capture conditions during a period of maximum biomass. The schedule of the 2016 IOPs was as follows:

IOP1 for Iowa (SMAPVEX16-IA): May 25 – June 5
IOP1 for Manitoba (SMAPVEX16-MB): June 8 – June 20
IOP2 for Manitoba (SMAPVEX16-MB): July 10 – July 22
IOP2 for Iowa (SMAPVEX16-IA): August 3 – August 16

The Passive/Active L-band Sensor (PALS) collected airborne data during these IOP windows and focused on the SMAP morning overpasses. Intensive field sampling was conducting during the IOPs; temporary soil moisture stations and tower-based radiometer/radar measurements bridged the gap between periods of intensive ground crew deployments.

6. Collection of Soil and Crop Data

During the two IOPs for SMAPVEX16-MB, soil and crop variables known to influence microwave emissions were targeted for measurement. These variables included soil moisture, surface and sub-surface soil temperature, surface roughness, as well as crop biomass, Leaf Area Index, phenology and water content. Both point based and field based reflectance measurements were also collected.

Crews were provided with a day of training prior to the commencement of the experiment. Sampling days were dedicated to either soil moisture or vegetation/surface roughness depending on whether aircraft flights took place (Table 3). During flight days, crews measured soil moisture and surface/sub-surface temperature on the 50 fields. During non-flight days crews measured surface roughness and crop parameters such as biomass, reflectance and Leaf Area Index. Down days were due to rain events or were used to give crews a rest. On soil moisture days, crews were deployed to the field at approximately 5:15 AM to allow for collection of soil moisture measurements coincident with the overpass time of SMOS and flight times of PALS.

Table 3. Dates for soil moisture, vegetation and surface roughness data collection

Soil Moisture	Vegetation	Roughness
June 8	June 13, 15	June 10
June 9*	June 18, 20	June 13
June 11	*June 27, 28***	June 15
June 14	*July 5, 6***	
June 16	July 11, 12	
June 19	July 17, 20	
June 20		
July 14		
July 16		
July 18		
July 19		
July 21		
July 22		

*No PALS flight

**Data collection between IOP campaigns. Half of the fields were sampled June 27-28; the other half July 5-6.

6.1 Soil Moisture Measurements Using Hand Held Hydra Probes

During SMAPVEX16-MB soil measurements were collected in each of the 50 agricultural fields, coincident in time to flight overpasses. A crew of two was tasked to measure soil moisture, surface and sub-surface soil temperature and surface vegetation temperature. Each crew was assigned four to five fields, typically arriving at their first field around 6:00 AM and finishing their last field before noon.

Crews were equipped with the Stephen's Hydra Probes (POGO) and an iPod with the HydraMon app installed (Figure 15). These probes are based on coaxial impedance dielectric reflectrometry and use an oscillator to generate an electromagnetic signal at 50 MHz that is propagated through three metal tines

into the soil. The part of the signal that is reflected back to the unit is measured in volts and is used to solve numerically Maxwell's equations to calculate the impedance and the real and imaginary dielectric permittivities. Real dielectric permittivity can be related to soil moisture using empirical relationships between dielectric and moisture or using physically based dielectric mixing models. The probes were inserted vertically into the soil, which provided dielectric and temperature measurements integrated over the top 5.7 cm of soil. Although readings were recorded digitally, crews were also asked to record soil moisture values on their field sheets. At the end of each day, data from the POGOs were downloaded and quality checked. Field sheets were scanned.

Figure 15. Hand held Stevens Hydra probe (POGO)

Each field crew were asked to sample moisture at 16 sample points in each field, as shown in Figure 14. At each sample point, crews were instructed to collect three replicate soil moisture measurements. Replication was important to capture spatial variability created by soil properties or management practices. Tillage and planting activities can create surface roughness, affecting surface soil moisture. If crews observed obvious surface roughness, they were instructed to distribute the three replicate measurements with the 1st reading between the crop plants at the top of a ridge, the 2nd reading in the middle of a ridge and the 3rd reading at the bottom of a ridge (Figure 16). In each position, the probe was to be inserted vertical to the surface and flush to the soil. If crews did not observe discernible structure, measurements were to be taken diagonally across rows, with the first reading close to the crop row. Crews noted on sampling sheets whether surface roughness was present.

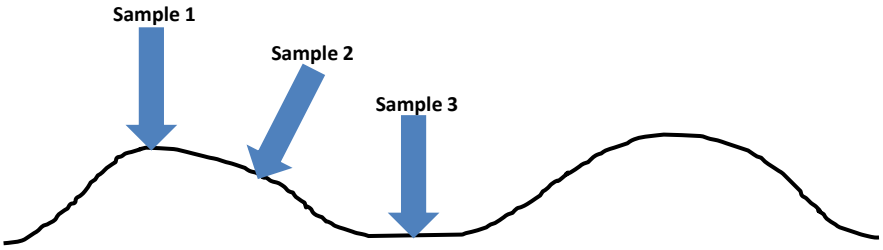

Figure 16. Location of replicate soil moisture measurements at each site

For the most part, field crews were successful in collecting data on all their assigned fields. However, on any given day some crews encountered circumstances preventing access to fields. This included poor road/field conditions, or aerial spraying of crops.

6.2 Soil Core Samples for Site Specific Calibration

Site specific calibration of measurements collected with the hand held probes is necessary. To assist with this calibration, during flight days crews were instructed to collect two bulk density cores per field. The first sample was always acquired at site 1, the location of the temporary in situ station in each field. The location of the second bulk density site was moved each flight day such that by the end of the campaign, one sample had been collected at most sample points within each field.

When the crew arrived at the designated bulk density sites for that particular sampling day, they took their three standard probe readings. As well, the crew collected a soil core and three additional probe readings. Volumetric soil moisture samples were taken using 5 cm aluminum rings (Figure 17). The ring was covered with a plastic cap and then pushed vertically down into the soil until fully inserted. Once the ring was fully inserted, the POGO was used to take three readings from the undisturbed soil surrounding the inserted ring. The POGO was carefully pushed in approximately 10 cm from the ring. Three real dielectric readings from around the ring were recorded using the HydraMon application. Once the POGO readings were completed, the samples (soil core and ring) were carefully dug out; excess soil around the ring was removed. The soil core (still in the ring) was placed in a tin with a lid, with the tin then being placed in a re-sealable plastic bag to minimize moisture loss. Soil cores were transported back to the University of Manitoba for weighing and drying. The entire sample (soil core, ring, tin, lid and bag) was weighed. The tin was then removed from the plastic bag, the lid was removed, and the base of the tin carrying the ring and soil core was placed in a soil drying oven. The samples were oven dried for 48 hours at 105^{o} C. Following drying, the entire sample (soil core, ring, tin) was then re-weighed. All samples of soil per field were retained for further soil analysis.

Figure 17. Soil core in the ground (left) and following removal (right)

The gravimetric moisture content was determined for each individual sample as the mass of water divided by the mass of oven-dry soil. In addition, the bulk density of each individual sample was determined as the oven-dry mass of soil divided by the aluminium ring volume. The average bulk density of all 26 calibration samples for each field determined the average bulk density of the surface soil for the entire field. The average bulk density was multiplied by the gravimetric moisture content of each individual sample to calculate the volumetric moisture content of each core sample. This approach follows the 2012 protocol in Rowlandson et al. (2013) which documented more accurate field-based calibrations using this method as opposed to using each individual sample's bulk density with each individual sample's gravimetric soil moisture content.

The volumetric soil moisture content for each core sample was used with the adjacent POGO reading to create a calibration equation. Volumetric water content is a linear function of the square root of real dielectric permittivity. As per Rowlandson et al. (2013), linear regression analysis was used to determine the equation of best fit between the volumetric moisture content (θ_V) and the square root of the dielectric permittivity (ε_{TC}) from the POGO as below:

$$\theta_V = a\,(\varepsilon_{TC})^{0.5} + b$$

6.3 Soil and Vegetation Temperature Measurements

Surface and sub-surface soil temperatures were also measured during flight days. Temperatures were recorded at four sites in each field (sites 1, 8, 9 and 16). Sub-surface soil temperatures were measured using a simple digital pocket thermometer (Figure 18). The digital thermometer was inserted to two depths, 5 cm and 10 cm. In addition, surface soil and vegetation temperatures were measured at these same four sites. In this case an Apogee IR Sensor was used (Figure 18). Crews recorded the temperature for sunlit vegetation and sunlit soil, as well as for shaded vegetation and shaded soil. During cloud cover it was not possible to acquire sunlit readings and thus not all sites have all four readings. All temperature measurements were recorded on the field sheets.

www.apogeeinstruments.co.uk

Figure 18. Temperature at 5 and 10 cm using a pocket thermometer (left) and at the surface using the Apogee IR sensor (right)

6.4 Surface Roughness

Macro and micro surface roughness are known to effect microwave emission and scattering. For agriculture fields, this roughness is primarily due to land management activities, modified over time by the effects of erosion by water and wind. Although the effects of land management on roughness can vary due to soil characteristics large roughness variations across a field are small. Consequently roughness was measured at only two sites in each field. In addition, the SMAPVEX16-MB campaign began after seeding and further effects due to management activity were not expected. As well, canopy closure reduced the influence of erosion forces. Thus roughness was measured only once. Roughness crews visited fields early in the campaign. For corn, bean and canola fields the presence of vegetation at the beginning of SMAPVEX16-MB was low (Figure 19b), facilitating the collection of roughness photos.

Information on surface roughness was gathered with a portable pin profilometer (Figure 19) that uses surface displacement and post-processing techniques to obtain root mean square roughness (rms) and roughness correlation length (ℓ). The pin boards are custom built, using metal pins with tips coated in red material, a wooden board, a set of legs to support the board and a mechanism to release pins for surface displacement. A metal bar is mounted on the board to hold a standard digital camera to take a picture of the roughness profile once it is in place. The board is one metre in length and the distance between the camera and the profiler is ~ 118 cm. Before taking the photo, if vegetation obstructed the view of the board the vegetation was flattened. As well, a bubble level on the pin profiler was used to level the board.

(a) (b)

Figure 19. Measuring surface roughness using the pin profiler
(a) Photographing displacement of pins due to surface roughness; (b) 1-metre profile over a corn field (#226) on June 10, 2016 during SMAPVEX16-MB

For each field, roughness measurements were collected at two sites. To adequately measure the correlation length, roughness measurements must be taken over long profiles (typically several metres). To achieve a longer 3-metre profile, once one profilometer measurement was taken, the instrument was moved such that the end of the first measurement became the start of the second measurement. This was repeated a second time to achieve a 3-metre profile comprised of three 1-metre profiles. The photographs of the three separate profiles were joined into a single profile using a matlab application, post data collection, to provide the two roughness parameters per site. For each site, the board should be placed parallel to the look direction of the SAR instruments (Sentinel-1 (descending), RADARSAT-2 (descending), TerraSAR-X (descending) and PALS flight) (Figure 20). However, since there is only 3-4° difference between the look direction of RADARSAT-2 in descending mode (282°) and those of Sentinel-1 (278.8° in descending mode) and TerraSAR-X (278° in descending mode), roughness measurements during SMAPVEX16-MB were made in the look directions of PALS and RADARSAT-2 (we disregarded the look directions of Sentinel-1 and TerraSAR-X). Therefore for each site a total of 6 photos (3 adjacent photos x 2 look directions) were taken. This led to 12 photos (3 adjacent photos x 2 sites x 2 look directions) for each field.

The look direction is the direction perpendicular to the orbital track or flight line. For RADARSAT-2 and Sentinel-1 and TerraSAR-X this is perpendicular to the descending orbital track. For PALS this is perpendicular to the flight track.

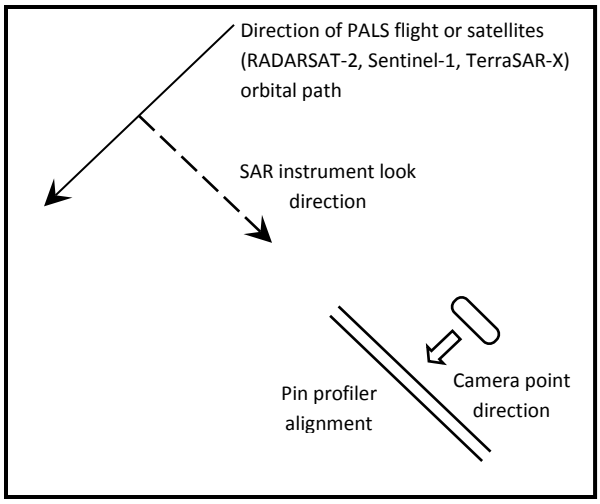

Figure 20. An example of the placement of the profilometer relative to look directions

A few exceptions should be noted. For a few fields (#82, 122 and 229), the roughness parameters at one of the two locations in the RADARSAT-2 look direction were extracted using a 2-m profile (instead of a 3-m profile), using 2 consecutive pictures. This occurred when the first or the third picture was of poor quality. These fields are highlighted in the roughness file.

For three other fields (#62, 71 and 226), the roughness parameters at one of the two locations in the PALS look direction were extracted using a 2-m profile (instead of a 3-m profile). Again, these were obtained using 2 consecutive pictures (when the 1st or the 3rd picture was of poor quality), and these fields are highlighted in the roughness file.

Finally, for field #82 the pictures taken at location 1 in PALS look direction were not processed due to their poor quality.

6.5 Crop Measurements and Biomass Sampling

6.5.1 Crop Density and Row Direction

Prior to the commencement of SMAPVEX16-MB, fields were visited to determine plant spacing, row spacing and row direction. Plant and row spacing are used to calculate plant density. Plant spacing was determined by counting the number of emergent plants in a row along a fixed distance of 1 meter. For each field, a small tennis ball was lobbed towards a random location on the field. At the spot where the tennis ball landed, the center of the meter stick was set down parallel to the closest row. The number of plants from one end of the meter stick to the other was counted. This was replicated for a total of 10 counts per field by moving perpendicular to the rows at each throw.

Row spacing was determined by measuring the distance between rows at each location where the plant counts were made. At each location after the plant counts, the meter stick was turned perpendicular to the row direction. At the soil level, the total distance was measured between the centers of the two plant rows immediately adjacent on either side of the row on which the plants were counted. The distance was divided by 2 to calculate average row spacing. The direction of planting was recorded (in degrees) using a compass, and using magnetic North as a reference.

6.5.2 Sampling Strategy for Crops

The sampling strategy for SMAPVEX16-MB was to collect crop data at three sites per field, at least once per week. The change in crop structure, biomass and water content is significant during this period of peak growth and thus weekly measurements were warranted. Three of the 16 soil moisture sites were selected for crop sampling. In 2012, sites 2 (on transect #1), 11 and 14 (both on transect #2) were selected. This worked well as transit time through the field was optimized and yet the distance between sites ensured that a range of crop conditions was sampled. This approach was also adopted in 2016 but with an adjustment to reduce the effect of trampling of crops around the soil moisture sampling sites; the crop sampling site was moved by one during the second week of each campaign window. As such, sites 2, 11, and 14 were sampled the first week of each IOP campaign window whereas sites 3, 10, and 13 were sampled the second week of each campaign window (Table 4).

Table 4. Location of the crop sampling sites for each week of the two field campaign windows.

IOP Campaign Window		Week	Dates	Sampling Sites
1	June 8 – 20	Week 1	June 8 – 13	2, 11, 14
		Week 2	June 14 – 20	3, 10, 13
2	July 10 – 22	Week 1	July 10 – 16	2, 11, 14
		Week 2	July 17 – 22	3, 10, 13

At each of these three sites, measurements of crop height were made. In addition biomass samples were collected and photos to measure Leaf Area Index (LAI) were taken. When clear sky conditions permitted, crop reflectance was measured at site 2 or 3 (depending on the week). Restricting reflectance measurements to one site was a result of the limitation in the memory capacity of the Crop Scan instrument. Due to different planting approaches of various crops, and the accumulation of crop biomass, the strategy to acquire crop measurements varied depending on crop type. For wheat, oats, canola and forage crops crews collected biomass and height measurements within a 0.5 m x 0.5 metre biomass square. All other crops have wide row and plant spacing and thus these measurements were taken along two adjacent plant rows.

6.5.3 Biomass and Vegetation Water Content

Crop biomass was collected via destructive sampling. Canopy or vegetation water content (VWC) can be derived from the biomass samples. One crop biomass sample was collected at each of the three sampling sites as listed in Table 4.

The approach to sample collection was determined by the crop (Table 5). For canola, wheat, oats and alfalfa, a 0.5 m x 0.5 metre square was placed over the canopy. All above ground biomass was collected by cutting all vegetation at the soil level within the square. For corn and beans fields, 5 plants along two rows (10 plants in total) were collected. Knowledge of the density of the crop permits scaling of these measurements to a unit area (m^2). Samples were placed first in a mesh bag, and then a plastic bag to minimize water loss prior to weighing the wet sample. At sites with significant biomass more than one bag was needed.

Table 5. Biomass sampling strategies for each crop type

Biomass Sampling Strategy	Crop Types
0.5 m x 0.5 m square	canola, wheat, oats, alfalfa
5 plants along two rows	corn, soybeans, black beans

Vegetation will degrade rapidly (beginning almost immediately) and thus weighing of the wet sample must be completed quickly. Thus during vegetation sampling days, the lab crew set up a temporary weighing station located on site. Field crews brought their vegetation samples to the portable lab station when possible and convenient. Wet weights were taken with the mesh bag remaining in the plastic bag. Following wet weighing, plastic bags were removed for drying of the sample.

The lab crew also partitioned specific samples by plant organs, i.e. from the sample at site 2 for week 1 and site 3 for week 2 of each IOP campaign window. There was an exception to this rule which is that all wheat/oat biomass samples were partitioned into (a) stems+leaves and (b) heads for all three biomass sites per field. The level of partitioning depended upon the crop and is described in Table 6. Alfalfa samples were not partitioned. After partitioning, samples were re-weighed to provide a wet weight by plant organ.

Table 6. Segmentation of the biomass sample by crop type

Crop	Site	Sample A	Sample B	Sample C	Sample D
Wheat, oats	Every site	Leaves / Stems			Heads
Corn	Site 2 or 3	Leaves	Stems	Tassels	Cobs
Canola, soybeans	Site 2 or 3	Leaves	Stems	Flowers	Seeds / Pods

When the plant samples were taken out of the plastic bags to be partitioned, they were subject to drying during the partitioning time period. Thus, the true wet weight of individual organs could not be determined and corrections were made to the wet weights of partitioned plant organs to account for moisture loss during partitioning. It was assumed that the rate of moisture loss was the same for all organs. The water loss from the wet weight of the whole plant sample in comparison to the amassed wet weight of the partitioned organs was assumed to be proportional to the total mass of each plant organ.

The mesh bags containing the plant samples were placed in the air drying facility at the University of Manitoba for approximately two weeks (Figure 21). Bags were periodically re-weighed to determine if air dry weights were stable. The bags were put back into the drying room until air dry weights remained unchanged, signaling that drying was complete. Air drying typically does not remove all of the crop water and thus samples were collected after air drying to determine an oven drying correction by crop type and growth stage. Here air dried sub-samples were ground to pass through a 2 mm sieve using a Wiley Mill, returned to the air drying room to stabilize for a minimum of 24 hours. Then air dried sub-samples were weighed then placed in an oven at 60o C for 48 hours before being re-weighed. This provided an oven-dry weight to air-dry weight correction for each sub-sample.

Figure 21. Mesh bags containing crop samples hanging in drying room at the University of Manitoba

It was observed that air dried subsamples that weighed < 3 g had extremely variable oven dry correction ranging from negative (i.e. they gained weight from oven-drying) to very high values compared to the majority of the dataset. Consequently, oven-dry samples less than 3 g were omitted from the oven-dry correction calculations. The remainder of the dataset was used to determine if a standard oven dry correction could be applied to all data. Two-tailed t-tests, assuming unequal variances, revealed that mean oven dry correction values of a crop's individual organs were statistically different (α= 0.05) from the mean value for all samples in the dataset, as well as the mean value of all samples in that specific crop. Therefore, a standard oven dry correction was applied to all samples of a particular crop's individual organs, using the mean oven dry correction for that organ.

6.5.4 Crop Height

Crop height can vary significantly and increasing the number of measurements improves the accuracy of the average crop height. Plants that were collected for the biomass sample were used for this measurement. In total 10 heights were measured, 5 in each of two rows for corn and soybean. For wheat, oats, canola and alfalfa the height was measured for 10 plants randomly selected within the biomass sampling square. Height was measured to the top of the upper most part of the canopy, whether leaf or fruit. Leaves were left in their natural orientation, and not extended, for this measurement.

6.5.5 Leaf Area Index (LAI)

LAI was measured with hemispherical digital photos. In this technique a camera with a fish eye lens captures photos of the crop canopy with the camera positioned at least 50 cm above or below the canopy. For SMAPVEX16-MB it was decided that all photos for all crops would be taken as downward facing. To facilitate standardization and ensure high quality photos, the camera was mounted on a telescopic light-weight aluminum pole (Figure 22). With these poles, cameras were suspended well above the crop canopy and a level fixed to the pole facilitated leveling of the camera.

.

Figure 22. LAI camera suspected over corn canopy (left) and fish eye photo of a soybean crop (right)

Seven photos were taken along two transects (14 photos in total) at each of the three sampling (Figure 23). Crews were instructed to take one photo then move approximately 5 metres to take the next photos. Field crews positioned themselves relative to the sun to minimize shadowing in the photos. These photos were post-processed to estimates of LAI using the CanEye software. All 14 photos were averaged to provide one estimate of LAI per sample site

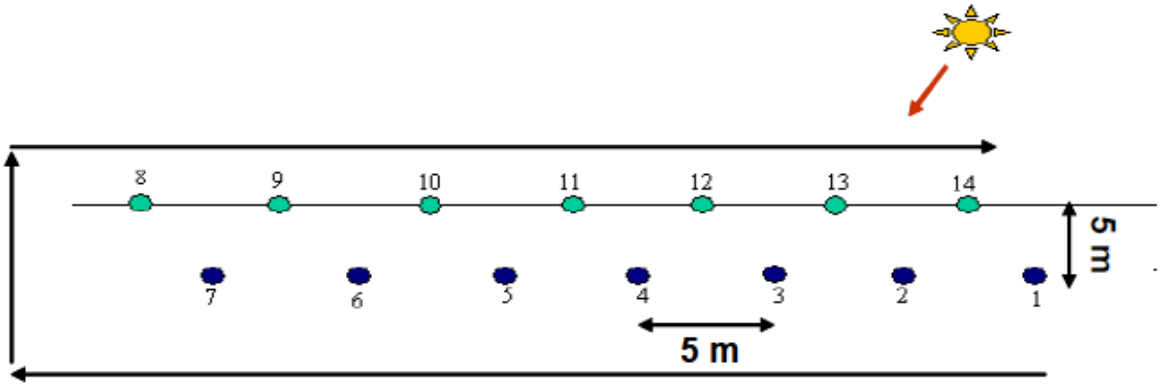

Figure 23. Sampling transect for hemispherical photos to measure LAI and CropScan

6.5.6 Crop Phenology

The lab crew was tasked with recording the phenology of each biomass sample for all 3 sample sites (Figure 24). When multiple bags of biomass were collected at a site, all bags were examined to determine consistency in phenology among samples. The BBCH (Biologische Bundesanstalt, Bundessortenamt and Chemical) scale was used to record phenology.

Figure 24. Staging crops at the portable lab (left) and wheat at infloresence emergence (right)

6.5.7 Point multi-spectral crop scans

Above canopy reflectance measurements were collected in order to characterize the general crop condition as measured at optical and infrared wavelengths using a CropScan multi-spectral instrument. The Crop Scan is a multispectral radiometer operating in 22 channels, ranging from 440 nm to 1700 nm. The radiometer has both upward and downward sensors to capture incoming solar radiation to the sensor and energy reflected from the canopy. These reflectance data were collected only at the first vegetation sample site (site 2 or 3 depending on the week) in a sub-set of fields. The crop scan measurements were taken at approximately the same points at which the LAI photos were captured (Figure 23). This yielded 14 crop scan measurements (7 in each of two rows) for one site in each measured field.

6.5.8 Field-scale multi-spectral crop scans

A drone-mounted Micasense RedEdge 3 multispectral camera (Figure 25) was used to acquire images along both transects on a subset of the sample fields on several dates during IOP 1 and 2. The camera acquires 5 spectral bands (Table 7). The spatial resolution of the camera images are less than 10 cm. A Before-Flight Reflectance Panel was used to capture a calibrated surface reading immediately before and after the flight on each field. The images were captured in the 5-hour period bracketing solar noon (approximately 1:30 p.m. Central Daylight Time) which is from 11:00 a.m. to 4:00 p.m.

Figure 25. Micasense RedEdge 3 multispectral camera

Table 7. Spectral bands captured by the Micasense RedEdge 3 camera

Band Number	Band Name	Center Wavelength (nm)	Bandwidth FMHM (nm)
1	Blue	475	20
2	Green	560	20
3	Red	668	10
4	Red Edge	717	10
5	Near Infrared	840	40

7. Ground-based Radiometer Measurements

Two L-band ground based radiometers (one from the Université de Sherbrooke (UdeS) and one from Environment Canada (EC)) were deployed during SMAPVEX16-MB. Two of the 50 SMAPVEX16-MB fields were selected for placement of the radiometers – one field of canola (# 202) and one field of wheat (#105) (Figure 26). These crop types were selected to complement a sister SMAPVEX16 campaign occurring in Iowa where radiometer and scatterometer measurements were collected over soybeans and corn.

Figure 26. Location of the microwave radiometers in the canola field (#202) (left) and wheat field (#105)

Both radiometers were installed at the edge of the fields to measure the surface (soil and vegetation) brightness temperature within the field (Figure 26). For the canola field, the radiometer was set up on the west side of the yard adjacent to the shelterbelt on the narrow grass strip between the trees and the canola. For the wheat field, the radiometer was positioned in the shelterbelt on the east side of the yard (Figure 27). At each location a 16 m half circle was flagged around the front of the radiometer, centred on the radiometer itself. This was marked out to prevent anyone from walking into the field of view of the radiometer's main -3 dB beamwidth at all multi-angular measurements or in any potential side lobe areas. The 16 m extent was determined by estimating the full -9 dB field of view of the EC radiometer positioned 2.75 m above ground with an incidence angle of 60 degrees. Both instruments were left in place from the beginning of the first SMAPVEX16-MB window to the end of the second window for the collection of continuous brightness temperature measurements at 40° incidence angle. When weather

permitted, daily multi-angular brightness temperature measurements were collected over the two fields during each window of the SMAPVEX16-MB campaign.

Figure 27. EC Radiometer deployed in field 202 (canola) (left) and UdeS radiometer deployed in field 105 (wheat) (right) on June 08, 2016

7.1 Description of Radiometers

Environment Canada (EC) L-band radiometer characteristics: This is an advanced dual polarized, hyperspectral L-band radiometer system built by Radiometrics Inc. The radiometer system observes emission within and around the reserved astronomy band of 1400 to 1427 MHz. The EC radiometer was designed with a bandwidth expanded outside the protected radio astronomy band with the intention of improving the ability to detect adjacent RFI-free channels. The 1375 to 1575 MHz bandwidth was chosen, with the upper limit determined by the availability of an appropriate analog-to-digital (A2D) sampler. Selected specifications of the EC L-band radiometer are provided in Table 8.

Table 8. EC L-band radiometer specifications

Component	Specification
Radiometer receiver architecture	High sideband down conversion
Frequency Range, GHz	1.40 to 1.55
Edge-to-edge IF bandpass, MHz	150 MHz (hyperspectral mode) or 25 MHz (broadband mode); user selectable
Hyperspectral mode	385 channels of 390.625 KHz width
Sensitivity, single observation 1 second delta T, Kelvins	0.61
Antenna HPBW, degrees	30
Sidelobes, -dB	-20
Type	Conformal Muffin Tin Antenna
Noise Figure, dB	3.6
Receiver noise temperature, Kelvins	374
Weight, kg	15 kg
Voltage, vdc	18 to 32
Power, watts maximum	100
Dimensions: antenna housing	60x57x42 cm
Environmental: temperature	-50 to +50C
Measurement specifications	
Calibrated Brightness Temperature Accuracy	~1.5K
Integration time	4.71 sec +/- 0.75 sec
Warm-up time (typical)	20 minutes

The angle of incidence of the antenna is adjusted manually with a hand-crank and a digital level, ranging from 30-70 degrees. For this campaign, the EC L-band radiometer was mounted to a mobile platform at a standard acquisition height of 2.50 m. This produced different footprint sizes which vary with the acquisition incidence angle (Table 9).

A RFI mitigation approach is applied to each polarization separately for all channels of EC radiometer within the 1400-1427 MHz spectrum. All subsequent temporal averaging of TB measurements is applied to the RFI mitigated data. The external instrument calibration uses two targets (sky, ambient) and the validation from independent stability measurements showed a mean absolute error (MAE) of 1.0 K for ambient and warm targets, while the MAE is 1.5 K for sky (Toose et al., 2016).

Table 9. EC Radiometer footprint size (meters) at various angles of incidence
The 40 degree incidence used for the long term continuous data acquisition is highlighted in yellow
(Toose and Roy, 2015)

Measured Angle (degrees)	Height Above Ground (meters)	Width	Depth
30	2.75	1	2
35		1	2
40		2	2
45		2	3
50		2	4
55		3	5
60		3	7

Université de Sherbrooke (UdeS) L-band radiometer characteristics: The UdeS L-Band radiometer is a dual polarization Potter Horn PR-1475 system built by Radiometrics Inc. (Boulder, Colorado). It is a high-gain, high-frequency receiver, outputting voltage through a square law detector making it proportional to receiver power. Peltier devices hold the receiver to a constant user-settable physical temperature, nominally +35C, to within about 0.03C for high receiver stability and accuracy. The PR-1475 is capable of receiving user-selectable bandwidths of 25 MHz or 150 MHz in the 1400-1550 MHz band. Selected specifications of UdeS L-Band radiometer are provided in Table 10.

Table 10. UdeS L-band radiometer specifications

Component	Specification
Radiometer receiver architecture	High sideband downconversion
Center frequency, GHz	1.475 or selectable
Edge-to-edge IF bandpass, MHz	150 or 25 MHz, user selectable
Sensitivity, single observation 1 second delta T, Kelvins	0.04
Antenna HPBW, degrees	30
Sidelobes, -dB	-23
Type	Potter horn
Noise Figure, dB	5.5
Receiver noise temperature, Kelvins	750
Weight, kg	10 kg
Voltage, vdc	22 to 32
Power, watts maximum	90
Warm-up time, minutes, from room temperature	30
Dimensions: receiver	38x14x25 cm with
Potter Horn	95x51 dia. cm
Environmental: temperature humidity	-50 to +50C 0 to 100% noncondensing
Measurement specifications	
Calibrated Brightness Temperature Accuracy	0.2 + 0.002*|Tref-Tsky| K
Long Term Stability	<1 K / 180 days
Resolution (depends on selected integration time)	0.1 to 1 K
Integration time (configurable)	10 – 2500 msec
Warm-up time (typical)	20 minutes

For this campaign, the angle of incidence of the antenna was adjusted manually with a hand-crank and a digital level, ranging from 30-70 degrees. The radiometer was mounted on two parallel ladders and the height of the radiometer (receiver in the Potter Horn) was set permanently at 2.50 m above ground, producing different footprint sizes which varied with the acquisition incidence angle.

For both UdeS and EC L-Band radiometers, Figure 28 provides approximate footprint sizes at multiple incidence angles. A soil pit station (see Section 7.2) was installed within the 40° footprint of both radiometers for the measurement of soil conditions.

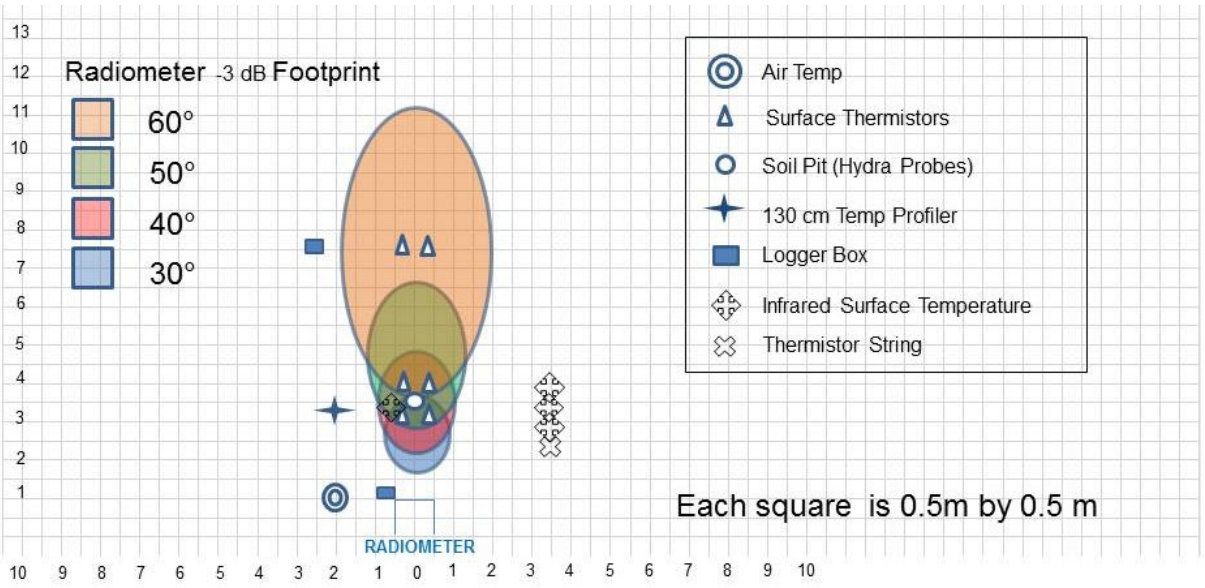

Figure 28. Approximate footprint size of the EC and UdeS surface-based radiometers
The approximate location of the hydra probes and instruments recording the soil and meteorological conditions in and around the footprint are provided.

7.2 Surface Characteristic Measurements For Ground Microwave Data Analysis

A temporary in situ station was installed inside the radiometer footprint (Figure 29) to collect soil moisture, soil temperature (1 Stevens Hydra Probe inserted vertically at the soil surface to collect integrated measurements over the 0-5.6 cm depth and 1 probe inserted horizontally at 5 cm) and air temperature measurements. These were supplemented with meteorological data and additional hand-held measurements. Each day the radiometer team collected soil moisture and surface temperature measurements at 8 points (x3 replicates) around the radiometer footprints. The same protocol for soil moisture, temperature and crop sample collection used for field crews to sample the 50 SMAPVEX16-MB fields was applied here.

Soil roughness was measured once during IOP Window 1; and crop biomass samples and height measurements were collect twice per week around the radiometer footprint.

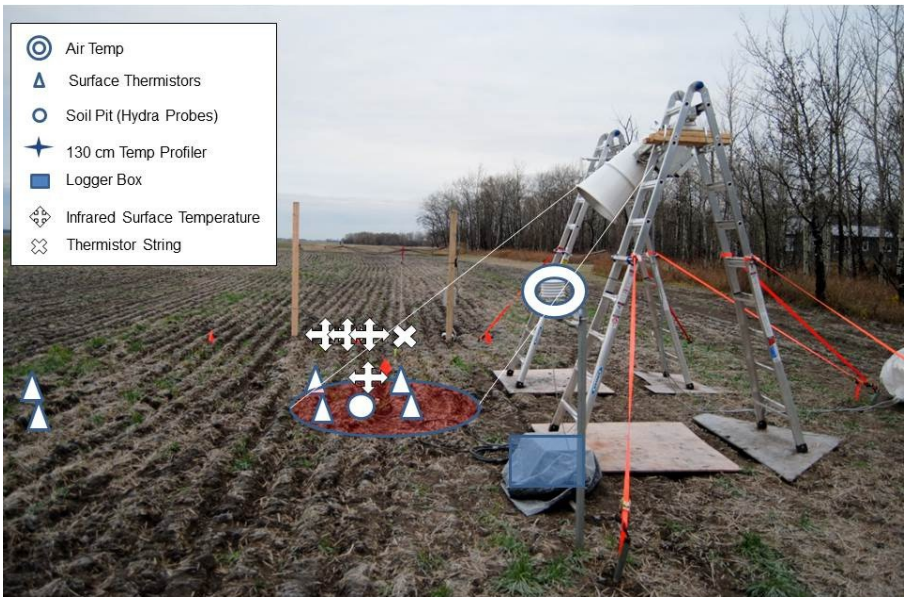

Figure 29. Approximate location of in situ sensors within the UdeS radiometer footprint.
The approximate footprint size of the -3 dB 40 degree footprint is illustrated with the red shaded ellipse (Toose and Roy, 2015).

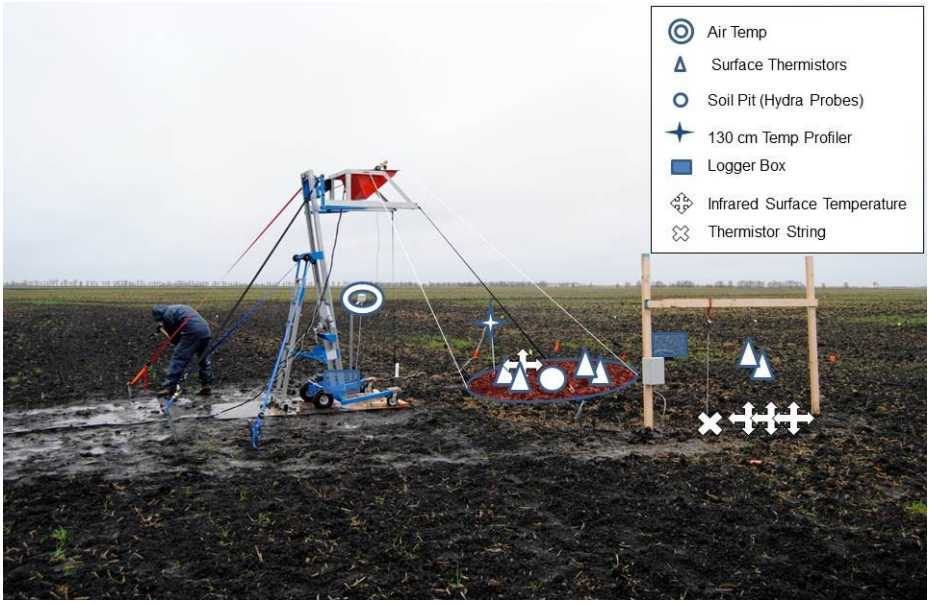

Figure 30. Approximate location of in situ sensors within the EC radiometer footprint.
The approximate footprint size of the -3 dB 40 degree footprint is illustrated with the red shaded ellipse (Toose and Roy, 2015).

7.3 Calibration Process

Prior to each multi-angular measurement calibration was conducted during the two IOPs to assure good stability of both radiometers. Several calibrations measurements were taken by using the sky (cold target) and Eccosorb (ambient target). No calibration was done for the continuous brightness temperature measurements collected between the two IOPs.

7.4 Continuous Brightness Temperature Measurements From L-band Radiometers

The measurements were collected between June 7th and July 21st, 2016. Brightness temperature measurements in horizontal and vertical polarizations (TBH and TBV) were acquired continuously at 40° incidence angle from the EC and UdeS L-band radiometers installed over a canola field (#202) and a wheat field (#105), respectively.

Original data were acquired continuously with an approximate 5 second integration time. The continuous data collection was only stopped to conduct regular routine calibrations, and to record the surface measurements at multiple angles between 30° and 70° with 5° increments (Section 7.2). In each instance, the radiometer's continuous measurements were halted for no more than 2 hours, and usually much less than this (20-30 minutes), to conduct calibration and multi-angular measurements. However, software issues led to missing data mostly at the beginning of the campaign for UdeS and at the end of the campaign for EC. Brightness temperatures have been averaged over 30 minute time steps to synchronize with in situ observations (soil moisture, temperature, air temperature) collected inside the radiometer footprint (Section 7.2).

7.5 Multi-angular Brightness Temperature Measurements From L-band Radiometers

When weather permitted, daily multi-angular observations of TBH and TBV from 30 to 70° with an increment of 5° (~ 1h30 per field) were collected on the canola and wheat fields in the morning during the two IOPs of SMAPVEX16-MB: June 8-20 and July 11-21, 2016. In addition, when SMOS PM acquisitions were available, multi-angular measurements were collected in order to analyze the diurnal variation of surface characteristics (crop, soil moisture) on the signal. These PM acquisitions were collected from both radiometers on June-10, June-13, June-16, June-18, Jul-14, Jul-17, Jul-19. A PM acquisition on Jul-11 was only available from the EC radiometer. At the same time as the PM brightness temperature acquisitions soil moisture, soil temperature and vegetation water content were measured.

7.6 Preliminary Analysis of Brightness Temperature Measurements

Figure 31 and Figure 32 show the temporal evolution of the calibrated TB measurements collected continuously at 40° from EC and UdeS radiometers, respectively as well as the *in situ* real dielectric constant (RDS) measurements made in and around the radiometer footprints. EC radiometer measurements show a clear respond to precipitation (Fig. 29) that can be related to very compacted soil at the edge of the field. This could lead to bad infiltration and liquid water at the soil surface (low T_B of liquid water). With UdeS radiometer measurements (Figure 30), we see a strong diurnal signal and a clear signal's depolarization at a late crop growth stage (due to increasing vegetation).

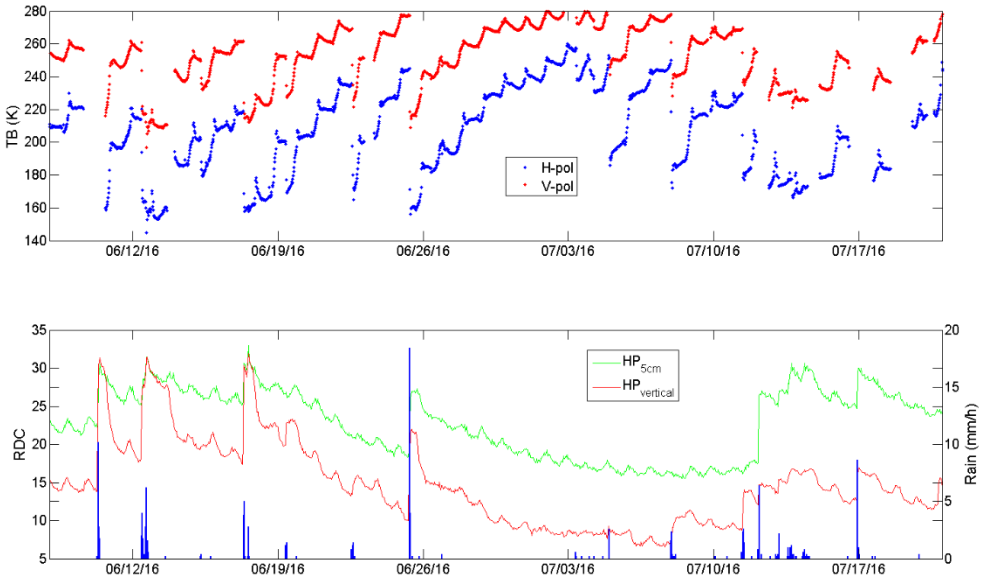

Figure 31. EC radiometer calibrated TB time series recorded continuously at 40° between June 8 and July 21, 2016

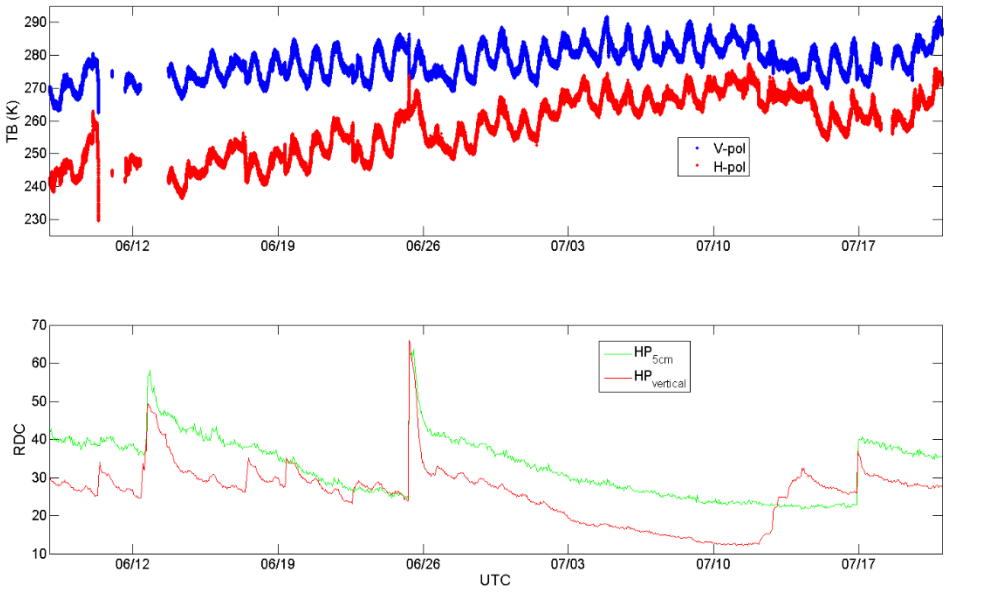

Figure 32. UdeS radiometer calibrated TB time series recorded continuously at 40° between June 8 and July 21, 2016

8. Data Collection by the Passive Active L-band Sensor (PALS) Instrument

The Passive Active L-band Sensor (PALS) provides radiometer products, vertically and horizontally polarized brightness temperatures, and radar products, normalized radar backscatter cross-section for V- transmit/V-receive, V-transmit/H-receive, H-transmit/H-receive, and H-transmit/V-receive. In addition, it can also provide the polarimetric third Stokes parameter measurement for the radiometer and the complex correlation between any two of the polarized radar echoes (VV, HH, HV and VH). Table 11 provides the key characteristics of PALS.

Table 11. Description of PALS

Instrument		Passive/Active L-band Sensor (PALS)
Owner		Jet Propulsion Laboratory (USA)
Platform		DC-3
Passive	Frequencies	1.413 GHz
	Polarizations	V, H, +45, -45 polarizations
	Spatial Resolution	20 degrees (3 dB beamwidth in Deg.)
Active	Frequencies	1.26 GHz
	Polarizations	VV, HH, VH, HV
	Spatial Resolution	20 degrees
Scan Type		360°
Antenna Type		Microstrip planar antenna with >30 dB polarization isolation
POC/Website		Simon.Yueh@jpl.nasa.gov

The planar antenna consists of 16 stacked-patch microstrip elements arranged in a four by- four array configurations. The measured antenna pattern shows better than 33 dB polarization isolation, exceeding the need for the polarimetric measurement capability. The antenna is shielded by a radome to allow conical scanning during flight.

PALS was mounted at a 40° incidence angle for a 360° conical scanning operation (Figure 31). The 3dB spatial resolution of the instrument was ~ 0.35*altitude above ground along-scan. PALS acquired data at two elevations during SMAPVEX16-MB (Low and High). The lowest elevation that PALS can operate at is determined by the minimum distance for radar data acquisition, which is 1067 m (3500 feet) AGL. The nominal elevation in this region is 305 m (1000 feet) ASL. Flight altitude for the low altitude flights was chosen to be 1200 m (about 4000 feet) AGL i.e. 1505 (about 5000 feet) ASL. The highest flight altitude for SMAPVEX was determined by the maximum where the instrument has operated without any issues (and for not requiring oxygen use by the flight crew); 3350 m (11000 feet) ASL, i.e., 3050 m (10000 feet) AGL. The spatial resolutions at these two flight altitudes are summarized in Table 12.

Figure 33. The PALS instrument mounted on the DC-3

Table 12. Geometric features of PALS data acquisitions

Target Altitude (m)	Nominal Ground Elevation (m)	ASL (m)	Along Scan Resolution (m)	Across Scan Resolution (m)	Effective Resolution (m)
1200	305	1505	581	777	595
3050	305	3355	1476	1974	1513

The PALS flight lines were designed to satisfy the major objectives of SMAPVEX16. Low altitude lines will be used to provide high spatial resolution data for fields/sites with homogeneous vegetation conditions. Sampling sites were located directly within the swath of these lines, to the degree possible. Since the nominal field size in the region is 800 m by 800 m, flying these at the low altitude (Table 12) provided the data necessary for field specific algorithm development and validation. Two lines were designed and the locations are listed in Table 13; they cover a range of agricultural conditions.

Table 13. PALS DC-3 Flight Plan

		START		STOP	
	Altitude AGL	Latitude (Deg.)	Longitude (Deg.)	Latitude (Deg.)	Longitude (Deg.)
Take off Winnipeg					
MB01	10,000 ft.	49.3618	-98.0881	49.7973	-98.0881
MB02	10,000 ft.	49.7973	-98.0275	49.3618	-98.0275
MB02	10,000 ft.	49.7973	-98.0275	49.3618	-98.0275
MB03	10,000 ft.	49.3618	-97.9668	49.7973	-97.9668
MB04	10,000 ft.	49.7973	-97.9062	49.3618	-97.9062
MB05	10,000 ft.	49.3618	-97.8455	49.7973	-97.8455
MBL01	4,000 ft.	49.7830	-97.9770	49.3700	-97.9770
MBL02	4,000 ft.	49.3700	-97.8970	49.7830	-97.8970
Return to Winnipeg					

The goal was to execute the flight plan on six SMAP overpass days during both IOPs. Go and no-go flight decisions were based primarily on readiness of the aircraft, weather conditions and surface conditions. If the aircraft was ready and weather conditions favourable, flights were a go as long as soil moisture conditions on the ground provided sufficiently different conditions relative to recent conditions. The intent was to capture a wide range of soil conditions, in particular those that follow rain events and subsequent dry down.

PALS flew six high altitude lines designed to map the SMAP pixel; two low altitude flight lines provided higher resolution data. A total of 12 soil moisture sampling days (6 in OIP 1 – June 8-20 and 6 in OIP – July 10-22) were completed during the campaign. During IOP1 PALS completed the flight plan on June 8, 11, 14, 16, 19 and 20, and during IOP2 the flights were completed on July 14, 16, 18, 19, 21 and 22. Figure X shows the horizontally polarized brightness temperature from the high-altitude flights. The overall difference in brightness temperature between IOP1 and IOP2 is due to the increased vegetation.

Point of contact for PALS:
Dr. Andreas Colliander
Terrestrial Hydrology Group, Jet Propulsion Laboratory
4800 Oak Grove Dr., M/S 300-320, Pasadena, CA 91109
Andreas.Colliander@jpl.nasa.gov

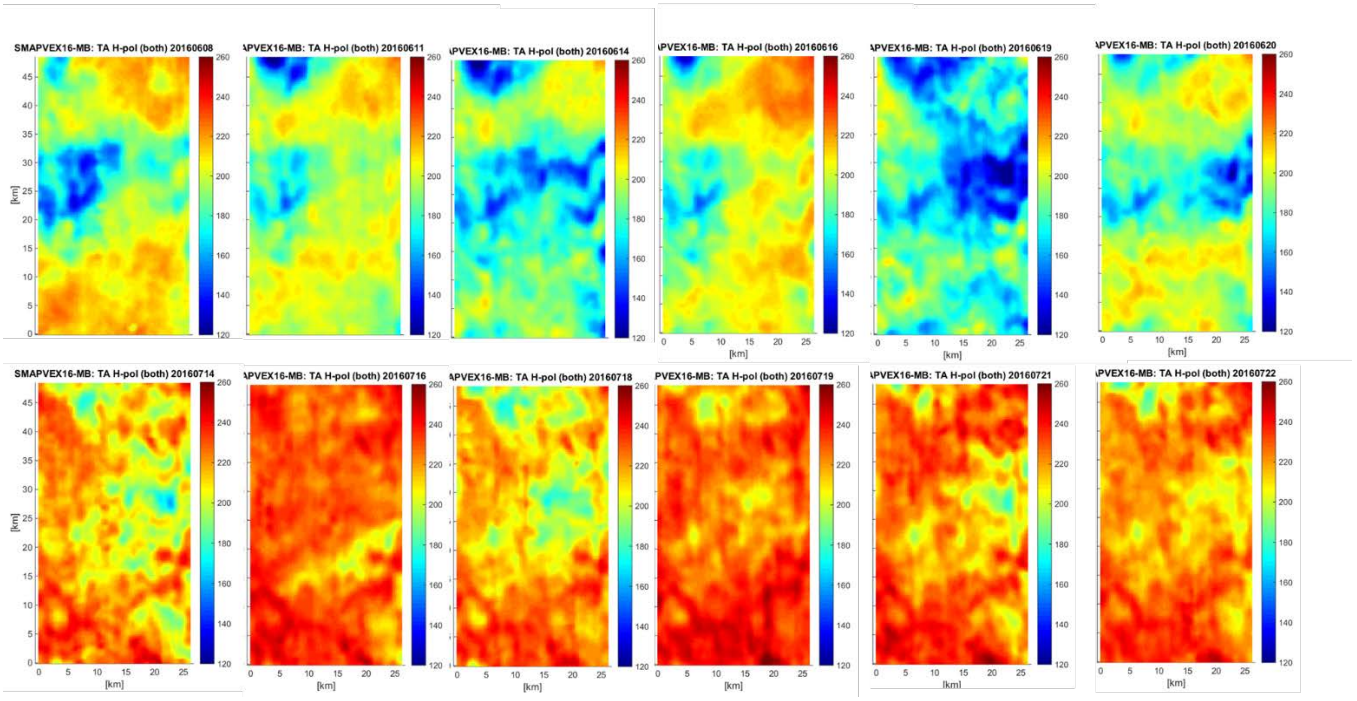

Figure 34. PALS horizontally polarized brightness temperature from the high-altitude flights for IOP1 (top row) and IOP2 (bottom row).
The overall difference in brightness temperature between IOP1 and IOP2 is due to the increased vegetation.

9. Satellite acquisitions

Both passive (SMAP and SMOS) and active (RADARSAT-2, Sentinel-1A/B, RISAT-1, TerraSAR-X, ALOS-2 PALSAR) microwave satellite data were collected before, during and after SMAPVEX16-MB. Landsat-8 and Sentinel-2 imagery was also available, and AAFC programmed acquisitions of RapidEye. The technical characteristics of these satellites are summarized in Table 14 and Table 15. For detailed descriptions, the reader is referred to the individual sensor web sites.

Table 14. Technical specification of satellites

Satellites	Frequency (GHz)	Polarization	Incidence angle (°)	Resolution
SMAP	1.41	V, H and U	40	40 km
SMOS	1.4	H and V	0 -55	30 km
Sentinel-1	5.405	VV+ VH, HH+HV, HH and VV	20 to 45	5-20 m
RADARSAT-2	5.4	Single Dual Quad	20-49	3-100 m
TerraSAR-X	9.65	Single Dual Quad	15 to 60	1-16 m
RapidEye				6.5 m
Sentinel-2				10-60 m

Table 15. Technical characteristics of optical sensors

Satellites	Spectral Band	Wavelength nm	Resolution
Landsat-8	Band 1 - Coastal/Aerosol	433 - 453	30
	Band 2 - Blue	450 - 515	30
	Band 3 - Green	525 - 600	30
	Band 4 - Red	630 - 680	30
	Band 5 - NIR	845 - 885	30
	Band 6 - SWIR	1560 - 1660	30
	Band 7 - SWIR	2100 - 2300	30
	Band 8 - Panchromatic	500 - 680	15
	Band 9 - SWIR - Cirrus	1360 - 1390	30
	Band 10 - LWIR	10300 -11300	100
	Band 11 - LWIR	11500 -12500	100
RapidEye	Band 1 - Blue	440 - 510	5
	Band 2 - Green	520 - 590	5
	Band 3 - Red	630 - 685	5
	Band 4 - Red Edge	690 - 730	5
	Band 5 - NIR	760 - 850	5
Sentinel - 2	Band 1 - Coastal/Aerosol	443-453	60
	Band 2 - Blue	458-523	10
	Band 3 - Green	542-578	10
	Band 4 - Red	650-680	10
	Band 5 - Vegetation Red Edge	697-712	20
	Band 6 - Vegetation Red Edge	732-747	20
	Band 7 - Vegetation Red Edge	773-793	20
	Band 8 - NIR	784-900	10
	Band 8A - Vegetation Red Edge	855-875	20
	Band 9 - Water Vapour	935-955	60
	Band 10 - SWIR - Cirrus	1360-1390	60
	Band 11 - SWIR	1565-1655	20
	Band 12 - SWIR	2100-2280	20

9.1 SMAP and SMOS coverage

SMOS: The Soil Moisture Ocean Salinity (SMOS) mission was launched in late 2009 by ESA. SMOS provides multiple polarization L-band brightness temperatures at multiple incidence angles. The mission also provides a soil moisture product. Spatial resolution of SMOS data is ~40 km. Products are posted on a 16 km grid (with 40 km resolution). Overpasses occur in the morning and evening with 16 ascending acquisitions and 16 descending acquisitions occurring during the intensive field campaign. The coverage during SMAPVEX is summarized in Table 16. Note that this has been restricted to passes with coverage closer to the center of the swath to improve data quality. Times are in local time. Details on SMOS and SMOS data can be found in Kerr et al. (2012).

SMAP: The Soil Moisture Active Passive (SMAP) mission is one of the first Earth observation satellites developed by NASA in response to the National Research Council's Decadal Survey. The SMAP satellite uses a combined L-band radiometer and radar instruments sharing a rotating 6-m mesh reflector antenna to provide high-resolution global maps of soil moisture at multiple spatial resolutions of 1 – 3 km. The incidence angle is 40 degrees. During SMAPVEX16-MB there were 16 ascending acquisitions, which occurred during the evening of the intensive field campaign and 16 descending acquisitions during the morning of the intensive field campaign. On July 7 2015, the SMAP radar stopped transmitting and was officially announced unusable on 2 September 2015. The mission continues with data being returned only by the radiometer. The coverage during SMAPVEX is summarized in Table 16 (O'Neill et al., 2013).

Table 16. Timing of SMAP and SMOS overpasses (LOCAL TIME)

	SMAP ASC		**SMAP DES**		**SMOS ASC**		**SMOS DES**	
Date (June)	Hour	Min	Hour	Min	Hour	Min	Hour	Min
6			8	14			19	54
7	19	20			7	12		
8	18	48	7	54	6	34	20	16
9			8	26				
10	18	32			6	56	20	38
11			8	2			20	0
12	19	9	8	37	7	18		
13	18	44			6	39	20	22
14			8	14			19	43
15	19	20			7	1		
16	18	57	7	49	6	23	20	5
17			8	26				
18	18	32			6	47	20	27
19			8	2			19	48
20	19	9	8	37	7	6		
21	18	44			6	28	20	10
22			8	14				
23	19	21			6	50	20	32
24	18	57	7	49			19	54
25			8	26	7	12		
26	18	32			6	33	20	16
27			8	2				
28	19	9	8	38	6	55	20	38
29	18	44					19	59
30			8	14	7	17		
Date (July)	Hour	Min	Hour	Min	Hour	Min	Hour	Min
1	19	20			6	39	20	21
2	18	57	7	49			19	42
3			8	26	7	1		
4	18	32			6	22	20	4

5			8	2				
6	19	9	8	37	6	44	20	26
7	18	44					19	48
8			8	14	7	6		
9	19	20			6	27	20	10
10	18	57	7	49				
11			8	26	6	49	20	32
12	18	32					19	53
13			8	2	7	11		
14	19	9	8	37	6	33	20	15
15	18	44						
16			8	14	6	55	20	37
17	19	20					19	58
18	18	57	7	49	7	16		
19			8	26	6	38	20	20
20	18	32					19	42
21			8	2	7	0		
22	19	9	8	37	6	21	20	4
23	18	44						
24			8	14	6	43	20	26

9.2 C-Band SAR Satellite Acquisitions

RADARSAT-2: Both RADARSAT-2 orbits (ascending and descending) were programmed for SMAPVEX16-MB. Ascending acquisitions occur at approximately 7:00 PM local time; descending acquisitions at approximately 8:00 AM local time. For many acquisitions, multiple frames of 2 or 3 were programmed to maximize the coverage of the SMAP cal/val pixel. 52 dates of fully polarimetric RADARSAT-2 were collected over the SMAPVEX16-MB site, eight of these dates overlapping with the intensive field campaign.

Table 17. RADARSAT-2 acquisitions (April-December 2016)
Shaded entries are acquisitions which occurring during intensive field campaign.

Date UTC	Time UTC	Date Local	Time Local	Orbit	Mode	Frames
Apr-04	12:53:03 PM	Apr-04	07:53:03 AM	DES	WideFQ (FQ8W)	3
Apr-05	12:15:41 AM	Apr-04	07:15:41 PM	ASC	WideFQ (FQ10W)	3
Apr-18	12:44:43 PM	Apr-18	07:44:43 AM	DES	WideFQ (FQ17W)	3
Apr-19	12:07:22 AM	Apr-18	07:07:22 PM	ASC	WideFQ (FQ2W)	2
Apr-22	12:19:50 AM	Apr-21	07:19:50 PM	ASC	WideFQ (FQ15W)	3
Apr-28	12:53:03 PM	Apr-28	07:53:03 AM	DES	WideFQ (FQ8W)	3
Apr-29	12:15:41 AM	Apr-28	07:15:41 PM	ASC	WideFQ (FQ10W)	3
May-12	12:44:45 PM	May-12	07:44:45 AM	DES	WideFQ (FQ16W)	3
May-13	12:07:20 AM	May-12	07:07:20 PM	ASC	WideFQ (FQ2W)	3
May-16	12:19:48 AM	May-15	07:19:48 PM	ASC	WideFQ (FQ15W)	3
May-23	12:15:39 AM	May-22	07:15:39 PM	ASC	WideFQ (FQ10W)	3

May-30	12:11:29 AM	May-29	07:11:29 PM	ASC	WideFQ (FQ7W)	3
Jun-06	12:07:20 AM	Jun-05	07:07:20 PM	ASC	WideFQ (FQ2W)	3
Jun-08	12:57:14 PM	Jun-08	07:57:14 AM	DES	WideFQ (FQ3W)	3
Jun-09	12:19:48 AM	Jun-08	07:19:48 PM	ASC	WideFQ (FQ15W)	3
Jun-12	12:40:35 PM	Jun-12	07:40:35 AM	DES	WideFQ (FQ20W)	3
Jun-15	12:53:04 PM	Jun-15	07:53:04 AM	DES	WideFQ (FQ7W)	3
Jun-22	12:48:54 PM	Jun-22	07:48:54 AM	DES	WideFQ (FQ11W)	3
Jun-23	12:11:29 AM	Jun-22	07:11:29 PM	ASC	WideFQ (FQ7W)	3
Jun-29	12:44:45 PM	Jun-29	07:44:45 AM	DES	WideFQ (FQ16W)	3
Jun-30	12:07:20 AM	Jun-29	07:07:20 PM	ASC	WideFQ (FQ2W)	3
Jul-02	12:57:13 PM	Jul-02	07:57:13 AM	DES	WideFQ (FQ3W)	3
Jul-03	12:19:48 AM	Jul-02	07:19:48 PM	ASC	WideFQ (FQ15W)	3
Jul-09	12:53:04 PM	Jul-09	07:53:04 AM	DES	WideFQ (FQ7W)	3
Jul-10	12:15:39 AM	Jul-09	07:15:39 PM	ASC	WideFQ (FQ11W)	3
Jul-16	12:48:54 PM	Jul-16	07:48:54 AM	DES	WideFQ (FQ11W)	3
Jul-17	12:11:29 AM	Jul-16	07:11:29 PM	ASC	WideFQ (FQ7W)	3
Jul-20	12:23:58 AM	Jul-19	07:23:58 PM	ASC	WideFQ (FQ20W)	3
Jul-23	12:44:45 PM	Jul-23	07:44:45 AM	DES	WideFQ (FQ16W)	3
Jul-24	12:07:20 AM	Jul-23	07:07:20 PM	ASC	WideFQ (FQ2W)	3
Jul-26	12:57:13 PM	Jul-26	07:57:13 AM	DES	WideFQ (FQ3W)	3
Jul-27	12:19:48 AM	Jul-26	07:19:48 PM	ASC	WideFQ (FQ15W)	3
Aug-02	12:53:04 PM	Aug-02	07:53:04 AM	DES	WideFQ (FQ7W)	3
Aug-03	12:15:39 AM	Aug-02	07:15:39 PM	ASC	WideFQ (FQ11W)	3
Aug-10	12:11:29 AM	Aug-09	07:11:29 PM	ASC	WideFQ (FQ7W)	3
Aug-17	12:07:20 AM	Aug-16	07:07:20 PM	ASC	WideFQ (FQ2W)	3
Aug-20	12:19:48 AM	Aug-19	07:19:48 PM	ASC	WideFQ (FQ15W)	3
Aug-27	12:15:39 AM	Aug-26	07:15:39 PM	ASC	WideFQ (FQ11W)	3
Sep-09	12:44:43 PM	Sep-09	07:44:43 AM	DES	WideFQ (FQ17W)	3
Sep-10	12:07:22 AM	Sep-09	07:07:22 PM	ASC	WideFQ (FQ2W)	3
Sep-12	12:57:12 PM	Sep-12	07:57:12 AM	DES	WideFQ (FQ4W)	3
Sep-13	12:19:50 AM	Sep-12	07:19:50 PM	ASC	WideFQ (FQ15W)	3
Sep-19	12:53:03 PM	Sep-19	07:53:03 AM	DES	WideFQ (FQ8W)	3
Sep-20	12:15:41 AM	Sep-19	07:15:41 PM	ASC	WideFQ (FQ10W)	3
Oct-03	12:44:43 PM	Oct-03	07:44:43 AM	DES	WideFQ (FQ17W)	3
Oct-04	12:07:22 AM	Oct-03	07:07:22 PM	ASC	WideFQ (FQ2W)	3
Oct-13	12:53:03 PM	Oct-13	07:53:03 AM	DES	WideFQ (FQ8W)	3
Oct-14	12:15:41 AM	Oct-13	07:15:41 PM	ASC	WideFQ (FQ10W)	3
Oct-27	12:44:43 PM	Oct-27	07:44:43 AM	DES	WideFQ (FQ17W)	3
Oct-28	12:07:22 AM	Oct-27	07:07:22 PM	ASC	WideFQ (FQ2W)	3
Nov-06	12:53:03 PM	Nov-06	06:53:03 AM	DES	WideFQ (FQ8W)	3
Nov-07	12:15:41 AM	Nov-06	06:15:41 PM	ASC	WideFQ (FQ10W)	3

Sentinel-1: The Sentinel-1 mission is a joint initiative of the European Commission (EC) and the European Space Agency (ESA). The payload of the satellite consists of a C-band SAR instrument with four exclusive imaging modes with different resolutions. Sentinel-1 provides dual polarization capability, very short revisit times and rapid product delivery. The use of Sentinel-1A and Sentinel-1B will assist with land monitoring of forests, water, soil and agriculture (Agency, Sentinel-1 User Handbook, 2013).

Both Sentinel-1A and 1B data were acquired in Interferometric Wide swath (IW) mode VV-VH polarization (Table 18). The Interferometric Wide swath (IW) mode combines a large swath width (250 km) with a moderate geometric resolution (5 m by 20 m). Observations from either satellite are on a 12-day repeat offset by 6-days. Acquisitions were as follows (bolded=1B).

Table 18. Sentinel-1A and Sentinel-1B acquisitions

Date UTC	Time UTC	Date Local	Time Local	Orbit	Mode	Look Direction	Status
June-13	12:15:30 AM	June-12	06:15:30 PM	ASC - 63	1A IW DV	Right	Available
July-13	12:14:41 AM	July-12	06:14:41 PM	ASC - 63	1B IW DV	Right	*
July-15	12:41:38 PM	July-15	06:41:38 AM	DES - 12	1A IW DV	Right	Available
July-18	12:22:59 AM	July-17	06:22:59 PM	ASC - 136	1B IW DV	Right	*
July-19	12:15:13 AM	July-18	06:15:13 PM	ASC - 63	1A IW DV	Right	Available
July-21	12:41:24 PM	July-21	06:41:24 AM	DES - 12	1B IW DV	Right	*

* In Orbit Commissioning Phase data. Available internally at ESA and JPL

RISAT-1: The RISAT-1 satellite acquired eight C-band images over the SMAPVEX12-MB site, four during the intensive campaign. These images were acquired in compact polarimetry mode, in both ascending and descending orbits and at right and left look directions.

Table 19. RISAT-1 acquisitions (May-August 2016)
Shaded entries are acquisitions which occurring during intensive field campaign.

Date UTC	Orbit	Mode	Look Direction
May-20	ASC	FRS-1 (RH/RV)	Right
Jun-08	DES	FRS-1 (RH/RV)	Right
Jun-14	ASC	FRS-1 (RH/RV)	Right
Jun-22	DES	FRS-1 (RH/RV)	Right
Jul-08	DES	FRS-1 (RH/RV)	Left
Jul-20	DES	FRS-1 (RH/RV)	Left
Aug-02	DES	FRS-1 (RH/RV)	Left
Aug-15	DES	FRS-1 (RH/RV)	Left

9.3 TerraSAR-X SAR Satellite Acquisitions

A TerraSAR-X proposal was approved by DLR. Under this proposal 18 TerraSAR-X images were acquired (ascending and descending) in dual stripmap mode (Table 20). There were five acquisitions during the intensive field campaign. Initially launched on 15 June 2007 TerraSAR-X is a German Aerospace Center and EADS Astrium joint venture created to provide more accurate SAR data in X-band. TerraSAR-X has multiple resolutions from 1m to 16m with an incidence angle of 15 to 60 degrees.

TerraSAR - X - Germany's radar eye in space. (2009, 07 08). Retrieved May 11, 2016, from DLR: http://www.dlr.de/eo/en/desktopdefault.aspx/tabid-5725/9296_read-15979/
http://www.dlr.de/eo/en/desktopdefault.aspx/tabid-5725/9296_read-15979/

Table 20. TerraSAR-X acquisitions (May-August 2016)
Shaded entries are acquisitions which occurring during intensive field campaign.

Date UTC	Time UTC	Date Local	Time Local	Orbit	Mode
May-14	12:20:37 AM	May-13	07:20:37 PM	ASC	stripNear_013
May-16	12:46:23 PM	May-16	07:46:23 AM	DES	stripNear_011
Jun-12	12:54:56 PM	Jun-12	07:54:56 AM	DES	stripNear_005
Jun-16	12:20:38 AM	Jun-15	07:20:38 PM	ASC	stripNear_013
Jun-18	12:46:24 PM	Jun-18	07:46:24 AM	DES	stripNear_011
Jun-23	12:54:57 PM	Jun-23	07:54:57 AM	DES	stripNear_005
Jun-27	12:20:39 AM	Jun-26	07:20:39 PM	ASC	stripNear_013
Jun-29	12:46:24 PM	Jun-29	07:46:24 AM	DES	stripNear_011
Jul-04	12:54:57 PM	Jul-04	07:54:57 AM	DES	stripNear_005
Jul-08	12:20:39 AM	Jul-07	07:20:39 PM	ASC	stripNear_013
Jul-10	12:46:25 PM	Jul-10	07:46:25 AM	DES	stripNear_011
Jul-19	12:20:39 AM	Jul-18	07:20:39 PM	ASC	stripNear_013
Jul-26	12:54:58 PM	Jul-26	07:54:58 AM	DES	stripNear_005
Jul-30	12:20:40 AM	Jul-29	07:20:40 PM	ASC	stripNear_013
Aug-06	12:54:59 PM	Aug-06	07:54:59 AM	DES	stripNear_005
Aug-10	12:20:41 AM	Aug-09	07:20:41 PM	ASC	stripNear_013
Aug-17	12:55:00 PM	Aug-17	07:55:00 AM	DES	stripNear_005
Aug-21	12:20:42 AM	Aug-20	07:20:42 PM	ASC	stripNear_013

9.4 ALOS-2 PALSAR Satellite Acquisitions

Four L-band PALSAR acquisitions occurred over the SMAPVEX16-MB site, although none during the intensive field campaign. These data were acquired in strip map mode (full polarization) (Table 21).

Table 21. ALOS-2 PALSAR acquisitions

Date UTC	Time UTC	Date Local	Time Local	Orbit	Mode	Frames
Jul-09	06:46:36 PM	Jul-09	01:46:36 PM	DES	SM2/FP6-6	2
Aug-06	06:46:36 PM	Aug-06	01:46:36 PM	DES	SM2/FP6-7	2
Aug-25	06:53:25 PM	Aug-25	01:53:25 PM	DES	SM2/FP6-3	3
Oct-01	06:46:36 PM	Oct-01	01:46:36 PM	DES	SM2/FP6-6	2

9.5 Optical Satellite Acquisitions

RapidEye: Acquisitions of RapidEye were programmed by AAFC for the SMAPVEX16-MB site, as a background mission. RapidEye is equipped with a 5 band, jena-optonik multi-spectral imager able to provide optical data from 440 – 850 nanometres.

LANDSAT: Landsat 8 is a joint NASA/USGS program that provides continuous acquisition and availability of Landsat data utilizing a two-sensor payload (operational land imager and thermal infrared sensor). Launched on February 11, 2013, it is the eighth satellite in the Landsat program. Landsat 8 measures Earth's surfaces in the visible, near-infrared, short wave infrared and thermal infrared, with a resolution of 15 to 100 metres. There will be 2 acquisitions which occurred during the intensive field campaign.

http://www.nasa.gov/mission_pages/landsat/overview/index.html

SENTINEL-2: Sentinel-2 is a European wide-swath, high-resolution, multi-spectral imaging mission. Sentinel-2 carries an optical instrument payload which samples 13 spectral bands. There are four bands at 10m resolution, six bands at 20m and three bands at 60m. The wavelength for the bands is from 443-2280nm. (Sentinel - 2 User Handbook, 2015)
https://earth.esa.int/documents/247904/685211/Sentinel-2_User_Handbook

Unfortunately most of the optical image acquisitions were obscured by cloud cover. Only those acquisitions with less than 50% cloud cover are listed in Table 22.

Table 22. Imagery acquisition dates for Landsat-8, RapidEye and Sentinel-2 sensors

Satellite	Date	Spatial Resolution	ROI Coverage	Cloud Conditions
Landsat-8	7/2/2016	30-m	~100%	~20%
Landsat-8	7/18/2016	30-m	~100%	~5%
Landsat-8	8/3/2016	30-m	~100%	~40%
RapidEye	5/19/2016	6-m	~100%	~0%
RapidEye	6/20/2016	6-m	~40%	~40%
RapidEye	7/4/2016	6-m	~95%	~5%
RapidEye	7/22/2016	6-m	~100%	~0%
RapidEye	8/16/2016	6-m	~60%	~5%
Sentinel-2	5/19/2016	10-m; 20-m; 60-m	TBD	TBD
Sentinel-2	5/26/2016	10-m; 20-m; 60-m	~100%	~10%
Sentinel-2	6/10/2016	10-m; 20-m; 60-m	TBD	TBD
Sentinel-2	6/21/2016	10-m; 20-m; 60-m	TBD	TBD
Sentinel-2	6/24/2016	10-m; 20-m; 60-m	~100%	~0%
Sentinel-2	8/2/2016	10-m; 20-m; 60-m	TBD	TBD
Sentinel-2	8/3/2016	10-m; 20-m; 60-m	TBD	TBD

10. References

Chan, S. K., R. Bindlish, P. E. O'Neill, E. Njoku, T. Jackson, A. Colliander, F. Chen, M. Burgin, S. Dunbar, J. Piepmeier, S. Yueh, D. Entekhabi, M. H. Cosh, T. Caldwell, J. Walker, X. Wu, A. Berg, T. Rowlandson, A. Pacheco, H. McNairn, M. Thibeault, J. Martínez-Fernández, Á. González-Zamora, M. Seyfried, D. Bosch, P. Starks, D. Goodrich, J. Prueger, M. Palecki, E. E. Small, M. Zreda, J. Calvet, W. T. Crow, and Y. Kerr. Assessment of the SMAP Passive Soil Moisture Product. IEEE Trans. Geosci. Rem. Sens., 54, pp. 4994-5007, 2016.

Kerr, Y.H., Waldteufel, P., Richaume, P., Wigneron, J.P., Ferrazzoli, P., Mahmoodi, A., Al Bitar, A., Cabot, F., Gruhier, C., Juglea, S.E., Leroux, D., Mialon, A., and Delwart, S. The SMOS Soil Moisture Retrieval Algorithm, IEEE Trans. Geosci. Rem. Sens, 50, pp. 1384-1403, 2012.

Ojo, E. R., Bullock, P. R., L'Heureux, J., Powers, J., McNairn, H., and Pacheco, A. Calibration and Evaluation of a Frequency Domain Reflectometry Sensor for Real-Time Soil Moisture Monitoring. Vadose Zone Journal, 14, 2015.

O'Neill, P., Entekhabi, D., Njoku, E., and Kellogg, K. The NASA Soil Moisture Active Passive (SMAP) Mission: Overview. NASA, 1-4, 2013.
http://ntrs.nasa.gov/archive/nasa/casi.ntrs.nasa.gov/20110015242.pdf

Rowlandson, T., Berg, A.A., Bullock, P.R., Ojo, E., McNairn, H., Wiseman, G., and Cosh, M.H. Calibration Procedures for Surface Soil Moisture Measurements during Soil Moisture Active Passive Experiment 2012 (SMAPVEX-12). Journal of Hydrology, 498, pp. 335-344, 2013.

Toose, P. and Roy, A. SLAP Freeze/Thaw Validation Experiment 2015 Surface-Based Radiometer Data Documentation, 2015.

Toose, P., Roy, A., Solheim, F., Derksen, C., Watts, T., Royer, A., and Walker, A.Radio frequency interference mitigating hyperspectral L-band radiometer, Geosci. Instrum. Method. Data Syst. Discuss., 2016. doi:10.5194/5194/gi-2016-27.

Appendix A. SMAPVEX16-MB participants

- **Aakash Ahamed,** NASA GSFC
- **Aaron Berg**, University of Guelph
- **Alexandre Roy,** University of Sherbrooke
- **Alicia Joseph**, NASA GSFC
- **Amine Merzouki**, Agriculture and Agri-Food Canada
- **Amirouche Benchallal,** University of Sherbrooke
- **Amy Unger***,* University of Manitoba
- **Anna Pacheco**, Agriculture and Agri-Food Canada
- **Andreas Colliander**, NASA JPL
- **Branden Wyryha,** Agriculture and Agri-Food Canada
- **Brynn Dagdick,** Agriculture and Agri-Food Canada
- **Chaima Touati,** ETE-INRS
- **Donvan Bangs,** University of Guelph
- **Erica Tetlock**, Environment Canada
- **Erle Einarsson**, Agriculture and Agri-Food Canada
- **Everlito Mendoza**, Province of Manitoba
- **Giuseppe Satalino,** ISSIA CNR
- **Hassan Bhuiyan,** Agriculture and Agri-Food Canada
- **Heather McNairn**, Agriculture and Agri-Food Canada
- **Ibrahima Barry,** University of Sherbrooke
- **Jarrett Powers**, Agriculture and Agri-Food Canada
- **Jenelle White,** University of Guelph
- **Juliette Lapeyre,** University of Sherbrooke
- **Krista Hanis,** University of Manitoba
- **Kurt Gottfried**, Agriculture and Agri-Food Canada
- **Kylie Roeland,** Agriculture and Agri-Food Canada
- **Manoj Kizhakkeniyil**, University of Guelph
- **Maria Abrahamowicz,** Environment Canada, Meteorological Research Division
- **Marla Riekman**, Province of Manitoba
- **Marliese Peterson,** Agriculture and Agri-Food Canada
- **Matt Gervais,** University of Manitoba
- **Matthew Friesen**, Agriculture and Agri-Food Canada
- **Mehdi Hosseini**, Agriculture and Agri-Food Canada
- **Mike Cosh**, USDA, ARS Hydrology and Remote Sensing Laboratory
- **Mitchell Krafczek,** Agriculture and Agri-Food Canada
- **Monique Bernier,** ETE**-**INRS
- **Paul Bullock,** University of Manitoba
- **Peggy O'Neill**, NASA GSFC
- **Ramata Magagi**, University of Sherbrooke
- **Rockford Bouchard,** Agriculture and Agri-Food Canada
- **Rotimi Ojo**, Province of Manitoba
- **Sab Kim**, NASA JPL
- **Stéphane Bélair**, Environment Canada - NWP and Data Assimilation
- **Tom Jackson**, USDA, ARS Hydrology and Remote Sensing Laboratory

- **Tracy Cummer**, Province of Manitoba
- **Tracy Rowlandson**, University of Guelph
- **Vineet Kumar,** Agriculture and Agri-Food Canada
- **Xiaoyuan Geng,** Agriculture and Agri-Food Canada